LAWRENCE
LIVERMORE
NATIONAL
LABORATORY

UCRL-JRNL-201505

Regional Heat Sources and the Active and Break Phases of Boreal Summer Intraseasonal (30-50 Day) Variability

H. Annamalai and K. R. Sperber

June 20, 2004

Journal of the Atmospheric Sciences

Disclaimer

Regional Heat Sources and the Active and Break Phases of Boreal Summer Intraseasonal (30-50 Day) Variability

H. Annamalai* and K. R. Sperber+

*International Pacific Research Center, University of Hawaii, Honolulu, Hawaii
+PCMDI, Lawrence Livermore National Laboratory, Livermore, California

Journal of the Atmospheric Sciences
June 2004
(Revised)

*Corresponding Author: Dr. H. Annamalai, IPRC/SOEST, University of Hawaii, 1680 East West Road, Honolulu, HI 96822, USA. Email: hanna@hawaii.edu

Abstract

The boreal summer intraseasonal variability (BSISV) associated with the 30-50 day mode is represented by the co-existence of three components, poleward propagation of convection over the Indian and tropical west Pacific longitudes and eastward propagation along the equator. The hypothesis that the three components influence each other has been investigated using observed OLR, NCEP-NCAR reanalysis, and solutions from an idealized linear model. The null hypothesis is that the three components are mutually independent. Cyclostationary EOF (CsEOF) analysis is applied on filtered OLR to extract the life-cycle of the BSISV. The dominant mode of CsEOF is significantly tied to observed rainfall over the Indian subcontinent. The components of the heating patterns from CsEOF analysis serve as prescribed forcings for the linear model. This allows us to ascertain which heat sources and sinks are instrumental in driving the large-scale monsoon circulation during the BSISV life-cycle.

We identify three new findings: (i) the circulation anomalies that develop as a Rossby wave response to suppressed convection over the equatorial Indian Ocean associated with the previous break phase of the BSISV precondition the ocean-atmosphere system in the western Indian Ocean and trigger the next active phase of the BSISV, (ii) the development of convection over the tropical west Pacific forces descent anomalies to the west. This, in conjunction with the weakened cross-equatorial flow due to suppressed convective anomalies over the equatorial Indian Ocean reduce the tropospheric moisture over the Arabian Sea, and promote westerly wind anomalies that do not recurve over India. As a result the low-level cyclonic vorticity shifts from India to southeast Asia and break conditions are initiated over India, and (iii) the circulation anomalies forced by equatorial Indian Ocean convective anomalies significantly influence the active/break phases over the

tropical west Pacific. Our model solutions support the hypothesis that the three components of the BSISV influence each other.

1. Introduction

During the Asian Summer Monsoon (ASM) season (June-September) there are two preferred locations of convection over the Indian longitudes, over the continent and over the equatorial Indian Ocean (Fig. 1a), often referred to as a bimodal structure in convection (Sikka and Gadgil 1980). These regions exhibit maxima in the variance of convection (Fig. 1b). The transition of convection from its oceanic to continental regime often involves intraseasonal northward propagation over India and the Bay of Bengal (Yasunari 1979; 1981; Krishnamurti and Subramanian 1982; Gadgil 1990). Similar north-northwestward migration of convection is also observed over the western Pacific (e.g., Murakami et al. 1984; Lau and Chan 1986; Chen and Murakami 1988; Wang and Rui 1990). These northward and northwestward propagating components coexist with the eastward propagating Madden-Julian oscillation (MJO) that is weaker in summer than in winter (Julian and Madden 1981; Hendon and Salby 1994). Collectively, these three propagating components dominate the intraseasonal variability during the ASM season (Gadgil and Asha 1992; Goswami 1994; Webster et al. 1998; Annamalai and Slingo 2001, hereafter referred to as AS01). Unless mentioned, throughout the present paper we refer to this intraseasonal signal, which has a time scale of 30-50 days, as the boreal summer intraseasonal variability (BSISV). The subseasonal variability of the ASM is also influenced by the 10-20 day mode and higher frequency synoptic systems (Gadgil and Asha 1992). However, in the present study we concentrate our analysis on the 30-50 day mode because it is associated with large-scale monsoon convective and circulation anomalies (AS01), and it explains more variance than the 10-20 day mode.

Over and above modulating the active and break phases of the ASM, the BSISV modulates the mean monsoon circulation (e.g., Krishnamurthy and Shukla 2000; Goswami and Ajayamohan 2001) and also the genesis of monsoon depressions over the Bay of Bengal and tropical cyclones

over the west Pacific (e.g., Liebmann et al. 1994; Goswami et al. 2003). Therefore, the statistical properties of the BSISV can influence the interannual variability of the ASM (Fennessy and Shukla 1994; Palmer 1994; Goswami 1994; Ferranti et al. 1997; Annamalai et al. 1999; Sperber et al. 2000; Krishnamurthy and Shukla 2000; Goswami and Ajayamohan 2001). Yet, current atmospheric general circulation models (AGCMs), when forced by observed sea surface temperature (SST), fail to simulate many aspects of the BSISV (e.g., Sperber et al. 2001; Kemball-Cook et al. 2002; Kang et al. 2002; Waliser et al. 2004). Thus, we seek a broader understanding of the interactions that give rise to the BSISV.

Several mechanisms have been proposed for the northward propagation of convection over the Indian and west Pacific longitudes. They include: (i) surface hydrology, (ii) air-sea interaction, and (iii) equatorial wave dynamics. While Webster (1983) emphasized the role of land surface heat fluxes in destabilizing the atmosphere ahead of the region of ascent, Goswami and Shukla (1984) stressed the importance of a convection-thermal relaxation feedback. Implementing some modifications to Webster's model, Gadgil and Srinivasan (1990) and Srinivasan et al. (1993) further highlighted the importance of hydrological processes. By incorporating the space-time variations in surface pressure, the model realistically simulated the persistence of the active phase over the Indian subcontinent (Nanjundiah et al. 1992). From an AGCM study, Ferranti et al. (1999) showed that feedbacks from the land-surface are not necessary for poleward propagation, but the variance associated with the BSISV enhances when the hydrology is interactive.

Both observations (e.g., Krishnamurti et al. 1988; Hendon and Glick 1997; Sperber et al. 1997: Sengupta et al. 2001; Kemball-Cook and Wang 2001; Hsu and Weng 2001; Woolnough et al. 2001; Vecchi and Harrison 2002; Sperber 2003) and coupled model experiments (e.g., Waliser et al. 1999; Kemball-Cook et al. 2002; Fu et al. 2003) indicate that at the intraseasonal time scale

positive SST anomalies lead the convection by about 10 days. This lead/lag relationship appears to be a critical factor in the organization and poleward migration of convection over the Indian longitudes (Fu et al. 2003). In AGCM's forced by SST, such a lead/lag relationship is absent and may account for the poor simulation of the BSISV (Waliser et al. 2004).

Lau and Peng (1990) show that as a result of the interaction of the large-scale monsoon flow with the equatorial Kelvin waves, unstable baroclinic Rossby modes are generated over the monsoon region at about 15-20^{o}N. Krishnan et al. (2000) suggest that forcing by dry (suppressed) convective anomalies over the Bay of Bengal leads to the development of low-level anticyclonic circulation anomalies as a Rossby wave response, which then propagate northwest to initiate the monsoon break over India. Lawrence and Webster (2002) show that the northward propagating convection is forced by surface frictional convergence into the low pressure center of the Rossby cell that is excited by equatorial convection. Wang and Xie (1997), Kemball-Cook and Wang (2001) and Jiang et al. (2004) point out that the emanation of Rossby waves is largely responsible for the northward migration of convection in the western Pacific and India. On the other hand, Hsu and Weng (2001) suggest that the combination of ocean-atmosphere interaction and circulation-convection interactions lead to the northwestward propagation in the western Pacific.

a. Quadrapole Structure in Convection

Figure 1c shows the variance explained by outgoing longwave radiation (OLR) at intraseasonal time scales during boreal summer. High variability is noticeable over (a) the equatorial Indian Ocean, (b) the northern Indian Ocean, including the Arabian Sea and the Bay of Bengal, (c) the northern tropical west Pacific, and to a lesser extent over (d) the equatorial west Pacific. Of the four regions, the northern tropical west Pacific exhibits the largest variance, though that over

the Arabian Sea is largest when expressed as a percent of the total variance (Fig. 1d). Consistent with the variance distribution, during its life cycle the convection associated with the BSISV depicts a "quadrapole" structure over the ASM domain (e.g., Lau and Chan 1986; Krishnan et al. 2000; AS01; also Fig. 2). Lau and Chan (1986) applied extended empirical orthogonal function (EEOF), and AS01 used Principal Oscillation Pattern (POP) analysis on filtered OLR and obtained the quadrapole structure, a north-south dipole over the Indian longitudes and a complementary pattern over the tropical west Pacific longitudes, and AS01 suggested that the quadrapole arises due to the co-existence of the three propagating components. Sperber et al. (2000) identified a similar pattern which was found to control the intraseasonal and interannual variations of the Indian summer monsoon. The quadrapole structure in convection is a robust feature, as will be further demonstrated in Section 3a.

Virtually all of the studies mentioned above examined the BSISV either over the Indian or over the west Pacific longitudes in "isolation". For example, it is known that the convective activity over the equatorial Indian Ocean modulates the active-break cycles over India (e.g., Sikka and Gadgil 1980), but it is unknown if the former influences the active-break cycles over the west Pacific. Additionally, the importance of the suppressed phase of convection to the life cycle of the BSISV is unclear.

b. Present study

Here, we will investigate whether the three propagating components of the BSISV influence each other. The null hypothesis is that they are mutually independent. We examine if the convective and associated circulation anomalies over the west Pacific longitudes exert considerable influence on the convective and circulation anomalies over the Indian longitudes and vice-versa. For

this purpose, we use reanalysis products, observed precipitation, a new diagnostic tool to capture the life cycle of the BSISV, and identify the relative impacts of local heating anomalies to the overall flow using an idealized model.

The paper is organized as follows: In Section 2 the data, the method used, and a brief description of the simple atmospheric model is given. Section 3 describes the observed characteristics of the BSISV, in terms of its evolution, air-sea interaction and Rossby wave dynamics and the relative role of the local heating anomalies to the overall flow obtained from the model solutions. Section 4 summarizes our conclusions.

2. Data, Method and Model

a. Atmospheric Data

The bulk of the atmospheric data used in our study is from the NCEP-NCAR reanalysis for the period 1979-95 (Kalnay et al. 1996). [This period was chosen to correspond with our previous intercomparison of summer monsoon in the NCEP-NCAR reanalysis and the European Centre for Medium-Range Weather Forecasts 15-year reanalysis (Annamalai et al. 1999). Additionally, this is the base simulation period of the Atmospheric Model Intercomparison Project (AMIP II) for which we will analyze summer monsoon variability in a subsequent paper.] The data assimilation and forecast model was implemented operationally at NCEP in January 1995. The model is run at a horizontal resolution of T62 and with 28 vertical levels. Upper air data on standard pressure surfaces have been supplied on a 2.5˚ latitude/longitude grid. Surface and 24-hour forecast fields (e.g., fluxes) are on the equivalent T62 Gaussian grid. Optimally interpolated SST of Reynolds and Smith (1994) were linearly interpolated to daily values.

The Advanced Very High Resolution Radiometer (AVHRR) OLR on the NOAA polar orbiting satellites has been used to identify the convective signature of the BSISV. These data have been daily averaged and processed on to a 2.5^{o} latitude/longitude grid with missing values filled by interpolation (Liebmann and Smith 1996). Intraseasonal variations of rainfall are characterized using the pentad-based Climate Prediction Center Merged Analysis of Precipitation (CMAP). This data set uses essentially the same algorithm and data sources as the monthly CMAP data set described by Xie and Arkin (1996).

b. Cyclostationary EOF's (CsEOF)

Some disadvantages in using POP analysis include fitting a sinusoidal function to the POP spatial patterns to obtain the life cycle of the BSISV (AS01), and in the case of EEOF analysis more than one EEOF and their corresponding Principal Component (PC) time series are needed to obtain the evolution of the BSISV (e.g., Lau and Chan 1986; Waliser et al. 2003). Additionally, the EEOF matrix subjected to analysis is overly large when using daily data since padding of lagged information is required. Since the CsEOF operates on the cyclicity of the covariance function, the space-time evolution is directly derived from the analysis (Kim and North 1997; Kim and Wu 1999).

Kim and Wu (1999) compared CsEOF analysis with other techniques commonly employed to extract space-time characteristics from geophysical time series such as EEOF, complex EOF, and POP. They found that CsEOF analysis captures the propagative features more realistically, in particular when the covariance of the given time series is cyclic in nature. For example, this technique has been successfully used to understand the propagative features of the ENSO (Kim and Wu 1999; Kim 2003).

CsEOF differs from standard EOF techniques in that it incorporates the “cyclicity” in the covariance function. Consider a time series in which the first two moment statistics, mean and covariance, are periodic with period “d1” and “d2”, respectively. The cyclicity in the mean represents, for example, the annual cycle (d1= 1 year) and can be removed from the data. The cyclicity in the covariance function indicates that the given time series is cyclostationary rather than a stationary one. The life cycle of the BSISV is approximately 40 days (Lau and Chan 1986; Lawrence and Webster 2002; AS01) and therefore taken as the cyclicity in the covariance function (d2 = 40 days). In CsEOF analysis d2 is called the “nested period”. Similar to standard EOF computations, CsEOFs are obtained as eigenfunctions of the cyclic covariance function, and the periodic time dependence of the Bloch functions (eigenfunctions) is due to the periodic time dependence of the covariance function. Therefore, instead of one spatial pattern as in EOF analysis, a Bloch function represents a series of spatial patterns for the nested period, d2.

The procedure for calculating CsEOFs involves three steps. First, a set of EOFs is constructed from the state space (original data) that retains more than 90% of the variance. Secondly, for the nested period of 40-days, the Bloch functions are constructed from the PC time series in temporal space. Finally, the Bloch functions are scaled by the EOFs to project the intended phenomenon in physical space. To preserve the cyclic stationarity in the covariance, the Bloch functions or CsEOFs repeat every nested period, and the PCs associated with them represent the low-frequency modulation of the Bloch functions and are known as the “stochastic undulation” (Kim 2003). Hence, the PCs of the CsEOFs are not the appropriate base time series to extract the coherent evolution of other variables. A different procedure is adopted here and explained in Section 3b. However, it is important to stress that the CsEOF spatial patterns that characterize the BSISV are important, so that we may ascertain the validity of our alternate approach.

c. Linear Baroclinic Model (LBM)

Linear models have been widely used as a diagnostic tool to elucidate the atmospheric response to idealized forcing (e.g., Matsuno 1966; Webster 1972; Gill 1980; Rodwell and Hoskins 1996; Watanabe and Jin 2002; 2003). In most cases the forcing, the anomalous diabatic heating is prescribed and the model's steady state response is sought. Linear models employed by previous studies to understand the dynamics associated with the BSISV (e.g., Wang and Xie 1997; Krishnan et al. 2000) have only 2 levels in the vertical (850 and 200 hPa) where the imposed heating is entirely projected on the first baroclinic mode. Wu et al. (2000) demonstrated that a single vertical mode approximation is incapable of approximating the qualitative 3-D structure of the response to tropical heating. Further, Mapes and Houze (1995) showed that the truncation of vertical modes greatly affects the amplitude of simulated low-level winds.

The model used here has been explained in detail by Watanabe and Kimoto (2000, 2001). Our configuration is similar to that used by Watanabe and Jin (2002). It is a global, time dependent, primitive equation model linearized about the climatology derived from NCEP-NCAR reanalysis for 1958-1997. The horizontal resolution is triangular truncation 21 and there are 20 vertical levels using the sigma (σ) coordinate system. Since the model has multiple levels, it is referred to as the linear baroclinic model (LBM), and it has the advantage of extracting all the vertical modes forced by the prescribed heating. The model employs diffusion, Rayleigh friction, and Newtonian damping with a time scale of 1 day^{-1} for σ levels greater than or equal to 0.9 and those less than or equal to 0.03, 5 day^{-1} and 15 day^{-1} for the fourth and fifth levels, while 30 day^{-1} is used elsewhere. Rayleigh friction coefficients represent not only friction but also other damping such as high frequency transient Reynolds stress (Wang 2004). The relatively weaker damping in the free atmosphere mimics nonlinearity in linear models (e.g., Ting and Yu 1998). To absorb ver-

tically propagating waves a common approach is to incorporate strong damping at the top of the models (e.g., Hendon and Salby 1996; Wu et al. 2000). In linear models, the equatorial wave responses to prescribed heating depends on the selection of the damping coefficients since the zonal distance that the signals can reach is characterized by the product of the damping time scale and the zonal group speed (Wu et al. 2000). The LBM results to be discussed are not sensitive qualitatively to the damping rate unless the damping is unrealistically small. The values we use at the model boundary layer are comparable or even stronger than that used by Wang Xie (1997) and Krishnan et al. (2000).

In the present study, the prescribed forcing is the anomalous diabatic heating proportional to the observed OLR (or precipitation) anomalies at various stages in the life cycle of the BSISV (Figs. 2 and 4). Lau and Peng (1987) and Sui and Lau (1989) showed that the zonal propagation speed of the forced signal is sensitive to the vertical structure of the prescribed heating. The vertical heating profile used is similar to that of Reed and Recker (1971) and has been employed in many previous studies (e.g., Rodwell and Hoskins 1996). To represent the top heavy heating associated with the BSISV (Mapes 2000), the maximum prescribed heating is at 400hPa (σ = 0.45). To maintain the divergence that promotes the baroclinic structure associated with MJO, Wang (2004) suggests that a minimum heating of ~2-3 mm/day of rainfall is necessary. In our case, for example, to mimic the positive heating over the equatorial Indian Ocean (Fig. 2d), the maximum heating imposed at 400hPa was 3^{o}K/day (18-20W/m^2 of OLR) or ~5 mm/day of rainfall (Fig. 4d). The horizontal shape of the heating is elliptical (e.g., Fig. 5a) and the heating is imposed on the summer (June to September) mean climatology derived from NCEP-NCAR reanalysis. Linearization about the zonally varying ambient flow (Section 3c) is considered. The LBM was integrated for 30 days with fixed forcing. With the dissipation terms adopted, the tropical response

approaches a steady state after day 10 and the response at day 20 is analyzed. Further, the heating amplitude used here is not crucial because numerical experiments show that the 3-D structure of the response is not sensitive to the amplitude of the heating as long as the maximum heating rate corresponds to less than 20 mm/day of precipitation (Wu et al. 2000).

3. Life Cycle of the BSISV

a. Cyclostationary EOF's

To isolate the variations related to the BSISV, the daily OLR has been bandpass filtered with a 20-100 day 100 point Lanczos filter. The CsEOF analysis is then applied to the filtered OLR over the ASM domain (30^{o}S-30^{o}N, 40^{o}E-180^{o}E) with a nested period of 40 days. It has been found that the leading CsEOFs are insensitive to the domain chosen.

Figure 2 shows the dominant CsEOF mode of OLR explaining 11.2% variance. Since the chosen nested period is 40 days, each panel in Fig. 2 is separated by 5 days. This CsEOF mode describes the life cycle of the BSISV and is consistent with the results presented in Lau and Chan (1986), and AS01. The space-time pattern clearly indicates that this mode is associated with northward propagation over the Indian longitudes and northwestward migration of convection over the tropical west Pacific. One major difference is that CsEOF analysis captures the west/ northwestward migration of the "convective maxima" associated with the Rossby waves over the Indian and west Pacific longitudes with more clarity than Wang and Xie (1997) and Lawrence and Webster (2002). The northward propagation occurs in conjunction with equatorial eastward propagation from the Indian Ocean to the west Pacific, characteristic of the MJO. One can easily delineate the co-existence of the three propagating components, and as such the intraseasonal modes are more complex during northern summer compared to northern winter. From observations

Lawrence and Webster (2002) found that 78% of the northward propagating events are accompanied with eastward propagating MJO. Although the domain averaged variance explained by CsEOF is modest, the maximum amplitude of OLR anomalies over the eastern Indian Ocean at day 0 (Fig. 2d) is in the order of 18-20 W/m^2.

b. Linear Regression and daily AIR variability

The CsEOF patterns in Fig. 2 give the life-cycle of convection based on the specification of an inherent 40-day periodicity. As discussed in Section 2b, each CsEOF pattern is associated with a low-frequency time series not appropriate for extracting covarying signals. In order to characterize the intraseasonal fluctuations, 20-100 day bandpass filtered OLR is projected onto the CsEOF pattern in Fig. 2d. This pattern, hereafter referred to as day 0, is chosen since it is also recovered as the dominant mode in a conventional EOF analysis (not shown). The resulting principal component time series, hereafter referred to as PC-4, is used for lagged linear regression. The regressions are calculated for lags of +/- 20 days. The regressed fields are then scaled by a one standard deviation perturbation of PC-4, and plotted where the regression attains at least 5% significance assuming each pentad is independent as in Sperber et al. (1997) and Sperber (2003).

Using filtered OLR, Lawrence and Webster (2002) constructed a regional time series by averaging the data over (0-5^{o}N, 85^o-90^{o}E). This regional index was used to regress against other variables, but did not reveal the covarying signals over the tropical west Pacific. Other studies (e.g., Kemball-Cook et al. 2002) show latitude-time Hovmoller plots averaged over certain longitudes to infer the poleward propagation. A benefit of the present analysis is that PC-4 represents the convective activity over the entire ASM domain.

To understand how faithfully PC-4 captures the active/break phases of the monsoon over the Indian subcontinent, we calculated the lag correlations (+/-25 days) of PC-4 with observed daily all-India rainfall (AIR) series. Prior to the calculation, the AIR series was smoothed by a 9-day running mean to suppress high frequency synoptic variability. For each year we checked the maximum positive correlation (R+) and the minimum negative correlation (R-), and have plotted the larger of the square of either R+ or R- in Fig. 3. Assuming 12 degrees of freedom (R>= |0.532|) the relationship is significant at the 5% level, particularly in the years when the BSISV is very active (e.g., 1979). Thus, the lagged linear regressions and the model solutions are expected to reflect the active/break phases over India. In an earlier study, Sperber et al. (2000) used a different analysis and noted the quadrapole structure in precipitation and its strong association with daily AIR for the years 1971-95 (Figs. 8c, 9, and Table 1 of their paper).

c) Linear regression and LBM solutions

Figure 4 shows the regressions of PC-4 against 850hPa winds and CMAP rainfall. The close agreement between the rainfall regressions and the CsEOF patterns in Fig. 2 indicates that the lagged regressions are faithfully capturing the life cycle of the BSISV. Overall, the 850hPa wind anomalies are dynamically consistent with the precipitation anomalies, and the lead/lag relationship among SST, convergence and convection are also present in the regressions (not shown for brevity). Briefly, the active phase of the Indian monsoon develops as the anomalous cyclonic circulation, in the form of Rossby waves, move north-northwestward. The equatorial rainfall enhancement moves into the western Pacific from day 0 to day 10 as the active monsoon over India matures (Figs. 4d-f). The active monsoon over India (Figs. 4f, g) is characterized by stronger cross-equatorial flow and cyclonic vorticity over the northern Indian Ocean. The extension of

convection into the western Pacific has been preceded by above-normal SST, and enhanced convergence and 850hPa moisture (not shown). As over the Indian monsoon region, cyclonic vorticity over the tropical west Pacific dominates during the active phase. A near mirror image in convection and circulation anomalies exists during the break monsoon phases. The observed features agree with recent studies (e.g., Krishnan et al. 2000; Sengupta et al. 2001).

Despite this close association between convection and circulation anomalies it is rather difficult to test the null hypothesis that the heat sources act independently using observed regressions alone. In an attempt to isolate cause and effect relationships between the various heat sources we utilize the LBM. By specifying the individual heatings in the LBM, we can ascertain which heat source (if any) is responsible for the total low-level wind response, and determine the relative importance of remote versus local teleconnection in the life-cycle of the BSISV. The amplitude of the wind anomalies from the LBM are, however, stronger than those in the regressions but are not expected to influence our interpretation since the magnitude of the response, but not the spatial pattern, is proportional to the strength of the imposed heating. The eight panels in Figs. 2 and 4 describe the entire life cycle of the BSISV and we obtained solutions for each of the heating anomalies in those panels. For brevity, we show the results at selected time lags that reveal new findings such as (a) initiation of convection in the western Indian Ocean (b) circulation anomalies forced by west Pacific convection on the active/break phases over India, and (c) how the convective anomalies over the equatorial Indian Ocean influence the active-break phases over tropical west Pacific.

1) Initiation of convection over the western Indian Ocean

At day -15 over the equatorial Indian Ocean, suppressed convection is the prominent feature (Figs. 2a, 4a) and at low-level twin anticyclones develop on either side of the equator. The LBM

solution for the negative heating in Fig. 5a indicates that these arise as a Rossby wave response to suppressed convection over the equatorial Indian Ocean (Fig. 5b). The southern hemispheric component is, however, weaker than its northern hemispheric counterpart due to the asymmetry in the mean flow (e.g., Wang and Xie 1997; Krishnan et al. 2000). The dominance of westerly wind anomalies to the east, and easterly wind anomalies within and to the west of the suppressed convection suggest a Rossby-Kelvin wave packet (e.g., Wang and Xie 1997).

Over the near-equatorial Indian Ocean (poleward of 2.5^{o}S) the mean climatological winds are westerlies (e.g., Annamalai et al. 1999) and the SST over the equatorial central-eastern Indian Ocean is > 28^{o}C, the threshold required for deep convection (Gadgil et al. 1984). The easterly wind anomalies there act against the mean westerly flow and reduce evaporation (Fig. 6b) which contributes to the development of positive SST anomalies (Fig. 6a). The SST variation is primarily due to changes in latent heat flux and to a lesser degree to changes in surface shortwave flux (not shown). The SST regression presented throughout are an underestimate of the actual anomalies. In-situ measurements during BOBMEX (e.g., Bhat et al. 2001) and SST from TRMM Microwave Imager (e.g., Sengupta et al. 2001; Vecchi and Harrison 2002) indicates that during strong BSISV events the peak to peak SST amplitude could be as large as 2^{o}C. The underestimate arises due to (1) the regression over a large number of intraseasonal events, and (2) observed monthly (weekly) averaged SST's were used as the boundary condition in the reanalysis prior (including and subsequent) to December 1981.

Near the African coast the convection associated with the next active phase of the BSISV begins (Figs. 4a and 4b). Convergence (negative divergence) anomalies are located immediately to the east of enhanced rainfall, especially near 5^{o}N on day -15 (Fig. 6c). This is accompanied by a build-up of 850hPa moisture (Fig. 6d). The model solutions in Fig. 5 illustrate that the easterly

anomalies over the equatorial Indian Ocean and convergence anomalies near the African coast are entirely forced by the equatorial Indian Ocean negative heating anomalies. Additional model experiments with stronger damping at low levels and reduced magnitude of the imposed heating do not alter the results presented in Fig. 5 and our conclusion that the Rossby wave response to the suppressed convection is instrumental in the onset of the next active phase of the BSISV. Sperber (2003) came to the same conclusion with regard to the onset of convection during the boreal winter MJO. From observations, Maloney and Hartman (1998) noted low level convergence and increase in tropospheric water vapor over east Africa at intraseasonal timescales when dry convective anomalies occur over equatorial Indian Ocean (their Figs. 3 and 4). In the present study, we have used a simple model to demonstrate the dominant role of suppressed convection in the initiation of next active phase.

Our findings at day -15 are also apparent during other portions of the BSISV life cycle. For example, when the monsoon is inactive over the tropical west Pacific (Figs. 4d-f) northeasterly wind anomalies prevail there that counteract the climatological flow, resulting in reduced evaporation (not shown) and positive SST anomalies (Fig. 7b). It is thus possible that over the ASM region, the suppressed phase of the convection preconditions the ocean-atmosphere system for the next active phase of the BSISV. We are currently examining this aspect in coupled general circulation models.

2) Active (dry) phase over the tropical west Pacific (equatorial Indian Ocean) and break initiation over India

Figure 7 shows the regressions and Figs. 8 and 9 show the model solutions for day 10 and day 20. At day 10 the winds over the Bay of Bengal recurve over northern India as cyclonic circu-

lation anomalies prevail there (Fig. 7a), and the model solution in Fig. 8a indicates that the positive heating over the Bay of Bengal gives rise to the cyclonic anomalies over India (see also Fig. 8d). The cross-equatorial moisture source and that over the Arabian Sea dominate the inflow into India (Fig. 7c).

By day 20 the cross-equatorial flow adjacent to Africa weakens and the available moisture at 850hPa over the Arabian Sea diminishes rapidly (Fig. 7f). The model solutions (Figs. 8, 9) are consistent with the regressions, and clearly demonstrate a significant reduction in the cyclonic vorticity over the Indian subcontinent from day 10 to day 20. With the transition to westerly anomalies over Indian and the Bay of Bengal by day 20, the monsoon trough over the Indian subcontinent collapses. The anomalous moisture signals over the Arabian Sea and southern Indian Ocean between 10^{o}S-20^{o}S at day 10 and day 20 are in agreement with the results of Cadet and Greco (1987) who investigated the moisture budgets during the active/break phases of the 30-50 day mode during the 1979 monsoon season. The model solution for negative heating over the equatorial Indian Ocean, Fig. 5b, indicates that the Rossby wave response dominates the low-level flow over the Indian Ocean, and extending from Saudi Arabia to the Bay of Bengal (Fig. 7d). This is borne out by the model solution (Fig. 5b) in which the response is manifested as an anticyclone that weakens the cross-equatorial flow, while that further north promotes dry air advection from Saudi Arabia, Iran, Afganistan, and Pakistan. These two factors limit the availability of precipitable water over the Arabian Sea (Fig. 7f). Dry-air advection was also noted by Sperber and Palmer (1996) in their analysis of the seasonal mean monsoon. A reduction in the moisture at upper tropospheric levels also occurs (not shown). Together, the lack of moisture influx by the cross-equatorial flow and the dry air advection results in the weakening of precipitation intensity over India

from day 10 to day 20, and additional moisture penetration into the western Pacific where the rainfall increases (Fig. 7d).

The westerly anomalies over India and the Bay of Bengal arise largely due to the Rossby wave response to the suppressed convection over the tropical Indian Ocean (Figs. 5a, 9a and 9b). The association of westerlies over the plains of northern India during the initiation of monsoon breaks has been noted by Raghavan (1973). However, the shift of the cyclonic vorticity from India at day 10 to southeast Asia is due to the positive heating over the tropical west Pacific (Fig. 9a). Even though the wind response due to the positive heating over the tropical west Pacific does not dominate the westerly response over India, it does contribute to the reduction in convection over India by forcing descent anomalies through the depth of the troposphere (Fig. 9c). The Rossby wave generation in the presence of convective heating dries the atmosphere to the west of convection through subsidence (Gill 1980; Rodwell and Hoskins 1996). The negative heating over the tropical Indian Ocean contributes to descent in the upper troposphere over India (Fig. 9c), suggesting that it helps cap off deep convection over India.

Bhat et al. (2001) speculated that the drying of the upper troposphere is due to forced descent anomalies. Raghavan (1973) also suggested that large-scale descent is one primary reason for the inhibition of convection during break phases. Bhat et al. (2001) and Rao et al. (2004) used BOBMEX data and satellite measurements, respectively, to show that the upper troposphere dries a few days before the commencement of monsoon breaks over India. This feature is also seen in Fig. 10 which shows the vertical cross-section of lead-lag regressions with specific humidity at 92.5^{o}E and averaged between 15^{o}N-20^{o}N. Apart from the fact that active (break) phases are associated with deep moist (dry) layer, consistent with other measurements, the upper troposphere dries well in advance before the break sets in. Despite uncertainties in the humidity data from

NCEP-NCAR reanalysis (e.g., Trenberth and Guillemot 1998) the results presented in Fig. 10 deserve attention. In summary, due to the co-existence of forced descent anomalies and drying from above, and reduced moisture due to weakened cross equatorial flow the rainfall over Indian and the Bay of Bengal decreases as the monsoon break initiates.

To gain some insight into the mechanisms and to assess the relative role of west Pacific versus equatorial Indian Ocean in initiating the break over India we show the evolution of the geopotential anomalies at 700hPa from the model solutions (Figs. 11 and 12). In the tropical west Pacific solution (Fig. 11), within 3 days of the imposed heating the *in situ* low pressure anomalies are well developed and are compensated by high pressure anomalies to the east and west. During the course of the LBM integration, the Kelvin wave component radiates eastwards, while the high pressure anomalies associated with the forced Rossby waves propagate westwards and cover the entire Indian subcontinent and Arabian Sea by day 6. As the low-pressure anomalies intensify over the tropical west Pacific, the Rossby waves continue to amplify attaining local height anomalies of >2 m over the Arabian Sea, and the pattern attains a steady-state by simulation day 12. The interpretations presented here have close similarity to those of Rodwell and Hoskins (1996).

In response to the equatorial Indian Ocean heating anomalies, the *in-situ* Kelvin-Rossby wave packet develops (Fig. 12a), with the high pressure anomalies over the equatorial Indian Ocean compensated by low pressure anomalies over the Maritime Continent. By simulation day 6, the symmetric Rossby waves over the Indian Ocean begin their westward journey, while the dry Kelvin wave generates high pressure anomalies over the Indonesian islands. During the evolution, the Northern Hemisphere Rossby wave response intensifies and attains a maximum amplitude of 1.5 m over the Arabian Sea by day 12. The Southern Hemisphere response weakens, primarily due to the asymmetry in the mean flow (e.g., Wang and Xie 1997; Krishnan et al. 2000). The

above normal pressure anomalies in the Northern Hemisphere are confined to southern peninsular India and the Arabian Sea. On the large-scale, the east-west pressure gradient between the Arabian Sea and tropical west Pacific favors a strong zonal component at low-level resulting in the weakening of relative vorticity over India.

From observations and a simple model, Krishnan et al. (2000) showed that northwest propagating Rossby waves, triggered by suppressed convective anomalies over the Bay of Bengal initiate a break over continental India. However, their mechanism becomes effective once dry convective anomalies get organized and spread over the Bay of Bengal (e.g., Fig. 4a at Day -15, or Figs. 4d-e of their paper). The LBM solutions presented here suggest that if one considers and extends the analysis to include the west Pacific and the effect of dry convective anomalies over the equatorial Indian Ocean at day 20 itself, the initiation of breaks over India can be diagnosed 5-10 days earlier.

3) Role of equatorial mode in the active-break phases over tropical west Pacific

The equatorial Indian Ocean heating also plays an important role for the amplification and reduction of convection over the tropical west Pacific. At day -15 the model solutions demonstrate that westerly wind anomalies forced by equatorial Indian Ocean suppressed convective anomalies extend zonally all the way into the west Pacific and strengthen the convergence and therefore the ongoing active phase there (Fig. 5b). When compared with the regression map in Fig. 4a, the model solutions clearly show that the low-level westerlies over the Bay of Bengal and north Arabian Sea are due to equatorial Indian Ocean convective anomalies and are not forced by west Pacific convective anomalies (compare Figs. 5b and c). In the opposite phase, the equatorial Indian Ocean forcing plays a role in the demise of the tropical western Pacific convection. Simi-

larly, when the monsoon is active over India the break phase over the west Pacific is amplified (Fig. 9a).

To gain some insight into how the equatorial mode influences the west Pacific monsoon, we return to Fig. 12. By day 3 of the LBM simulation, the below normal pressure over the Maritime Continent contains an eastward moving Kelvin wave and westward propagating symmetric Rossby waves. During its evolution, the Kelvin wave signal continues to radiate eastwards while the Rossby wave propagates north-westwards over tropical west Pacific. By day 12 over south China Sea the local anomalies are ~1.5 m. In a theoretical study, Lau and Peng (1990) showed that during northern summer, when the equatorial Kelvin waves reach the monsoon region in the vicinity of 140^{o}-150^{o}E, unstable baroclinic Rossby modes are initiated at about 15-20^{o}N. The geopotenial perturbations in Fig. 12 are consistent with their results. In addition, under the presence of mean vertical easterly shear, these Rossby waves are confined to the lower troposphere and they influence the low-level convergence (Wang and Xie 1996). This interaction only occurs when a zonally varying mean flow is prescribed in the model. When zonal mean flow is prescribed the growth of Rossby waves over the monsoon region is inhibited (figures not shown) consistent with the suggestion of Lau and Peng (1990) and Wang and Xie (1997).

4. Discussion and Summary

The BSISV is represented by the co-existence of three components, the poleward propagation of convection over the Indian and tropical west Pacific regions and eastward propagation along the equatorial Indian and west Pacific Oceans (Fig. 2). In the present study we investigate whether the three propagating components mutually influence each other using observational data and solutions to local heating anomalies from an idealized model. The null hypothesis is that the three com-

ponents are independent. Linearization about the zonally varying mean flow (Section 3c) is considered. Our focus is on the active/break cycles associated with the 30-50 day mode only.

The space-time evolution of the BSISV was extracted using CsEOF analysis on filtered OLR (Fig. 2). The dominant CsEOF mode explains 11% of the 20-100 day bandpass filtered domain averaged variance and describes the life cycle of the BSISV in a manner consistent with the previous results (e.g., Lau and Chan 1986; AS01). One important difference is that CsEOF extracts the west/northwestward migration of the "convective maximum" associated with the Rossby waves over the Indian and west Pacific longitudes with more clarity. The base PC time series of OLR, used for linear regressions against ocean-atmosphere variables, is significantly related to the daily observed rainfall over India (Fig. 3). The role of Rossby wave dynamics in the active-break phases over India (e.g., Krishnan et al. 2000; Lawrence and Webster 2002) and the tropical west Pacific (e.g., Hsu and Weng 2001) are also supported by the linear regressions and solutions from a linear baroclinic model. These model solutions have enabled us to isolate which regional heat sources contribute most strongly to the prevailing convective anomalies, and are therefore suggestive of a cause and effect relationship that otherwise could not be ascertained form the regressions alone.

Our findings indicate that at day -15 both regression and model solutions (Figs. 5, 6) show that the low-level easterly wind anomalies over the near-equatorial Indian Ocean act against the mean flow and reduce evaporation, and warm the sea surface over the equatorial western Indian Ocean. Subsequently, near the African coast the convection associated with the next cycle of the BSISV begins with 1000hPa convergence anomalies accompanied by an increase of 850hPa moisture. The model solutions unequivocally demonstrate that the low-level wind anomalies responsible for the initiation of convection is the Rossby wave response to suppressed convection

from the previous break phase of the BSISV (Fig. 5). Regression analysis and model solutions indicate that the circulation anomalies forced by suppressed convective anomalies warm the SST over the entire monsoon domain (e.g., Figs. 6b, 7b).

From day 5 to day 15, the active monsoon over India is associated with a stronger cross equatorial flow and abundant moisture at 850hPa over the Arabian Sea (Figs. 4, 7). As the active monsoon over India matures, the enhanced rainfall moves from the equatorial Indian Ocean to the western Pacific from day 0 to day 10. As the convection intensifies and moves poleward on days 15 and 20 (Fig. 7) over the west Pacific, it weakens over the Indian subcontinent. The enhanced convection over west Pacific forces descent anomalies over India (Fig. 9). At the same time, wind anomalies forced by the strengthening of dry convective anomalies over the equatorial Indian Ocean reduce the cross-equatorial flow and the available moisture at 850hPa over the Arabian Sea reduces rapidly (Figs. 7). Based on the model solutions we conclude that the circulation anomalies forced by enhanced (suppressed) convection over the tropical west Pacific (equatorial Indian Ocean) help trigger the break (active) phase over India. The long lead time noted here can be exploited in forecasting the monsoon break over India.

The model solutions indicate that the circulation anomalies forced by equatorial Indian Ocean convective anomalies play a role in the active and break phases over the tropical west Pacific. For example, at day 20 or day -15 (Figs. 5b, 12) the low-level westerly wind anomalies over the northern Indian Ocean extending into the tropical west Pacific enhance the convergence and amplify the convection in the latter region. In summary, based on the LBM results the null hypothesis that the three components of the BSISV are independent is rejected.

The results are constrained by linear solutions to prescribed heating rather than employing an interactive or moving heat source. In addition, the non-linearity between SST and convection,

over the warm pool has not been considered. In spite of these limitations, the results presented here require that the regional aspects of the heating anomalies need to be understood for a realistic simulation of the BSISV. Furthermore, possible teleconnections during the life-cycle of the BSISV, including the signals over Australia (e.g., Fig. 7b) will be investigated in a future study.

Acknowledgements: The authors express their gratitude to Dr. Masahiro Watanabe for providing the linear model and offering many useful suggestions on its use. Dr. Yoo Yin Kim is thanked for the cyclostationary EOF routine. Dr. Rupakumar, Indian Institute of Tropical Meteorology provided the daily AIR timeseries. Drs. Brian Mapes, Ragu Murtugudde, P.V. Joseph, Masahiro Watanabe, and Xianan Jiang are acknowledged for comments on the draft version of the manuscript. This research is partly funded by the Japan Agency for Marine-Earth Science and Technology (JAMSTEC) through its sponsorship of the International Pacific Research Center (IPRC). K. R. Sperber was supported by the U.S. Department of Energy, Office of Science, Climate Change Prediction Program at the University of California Lawrence Livermore National Laboratory under contract W-7405-ENG-48. Comments from the anonymous reviewers helped improve the manuscript. This is IPRC contribution XXXX and SOEST contribution YYYY.

References

Annamalai, H., J.M. Slingo, K.R. Sperber and K. Hodges, 1999: The mean evolution and variability of the Asian summer monsoon: comparison of ECMWF and NCEP/NCAR reanalyses. *Mon. Wea. Rev.,* **127,** 1157-1186.

--------, and --------, 2001: Active/break cycles: Diagnosis of the intraseasonal variability over the Asian summer monsoon. *Climate Dyn.,* **18,** 85-102.

Bhat, G.S., and Co-authors, 2001: BOBMEX: The Bay of Bengal Monsoon Experiment. *Bull. Amer. Meteor. Soc.,* **82,** 2217-2243.

Chen, T-C., and M. Murakami, 1988: The 30-50 day variation of convective activity over the western Pacific region with the emphasis on the northwestern region. *Mon. Wea. Rev.,* **116,** 892-906.

Fennessy, M.J., and J. Shukla, 1994: GCM simulations of active and break monsoon periods. Proc. of the Intl. Conf. on monsoon variability and prediction. Trieste, Italy. WCRP-84, WMO/TD-No. 619, Vol. 2

Ferranti, L., J.M. Slingo, T.N. Palmer and B.J. Hoskins, 1997: Relations between interannual and intraseasonal monsoon variability as diagnosed from AMIP integrations. *Quart.J.Roy. Meteor. Soc.,* **123,** 1323-1357.

----------, ----------, ----------, and --------, 1999: The effect of land surface feedbacks on the monsoon circulation. *Quart. J. Roy. Meteor. Soc.,* **125,** 1527-1550.

Fu, X., B. Wang, T. Li, and J.P. McCreary, 2003: Coupling between Northward-Propagating, Intraseasonal Oscillations and Sea Surface Temperature in the Indian Ocean. *J. Atmos. Sci.,* **60,** 1733-1753.

Gadgil, S., P.V.Joseph, and N.V. Joshi, 1984: Ocean atmosphere coupling over monsoon regions. *Nature,* **312,** 141-143.

--------, 1990: Poleward propagation of the ITCZ: observations and theory. *Mausam,* **41,** 285-290.

-------, and S. Srinivasan, 1990: Low frequency variations of tropical convergence zones. *Meteor. Atmos. Phys.,* **44,** 119-132.

--------, and G. Asha, 1992: Intraseasonal variation of the summer monsoon I: observational aspects. *J. Meteor. Soc. Japan,* **70,** 517-527.

Gill, A.E., 1980: Some simple solutions for heat-induced tropical circulation. *Quart. J. Roy. Meteor. Soc.,* **106,** 447-462.

Goswami, B.N., and J. Shukla, 1984: Quasi-periodic oscillations in a symmetric general circulation model. *J. Atmos. Sci.,* **41,** 20-37.

--------., 1994: Dynamical predictability of seasonal mean rainfall: problems and prospects. *Proc. Indian. Natl. Sci. Acad.,* **60A,** 101-120.

---------, and R.S. Ajaya Mohan, 2001: Intraseasonal oscillation and interannual variability of the Indian summer monsoon. *J. Climate,* **14,** 1180-1198.

---------., ----------, Prince K Xavier and D. Sengupta, 2003: Clustering of low pressure systems during the Indian summer monsoon by intraseasonal oscillations. *Geophys. Res. Lett. 30(8),*1431, doi:10.1029/2002GL016734, 2003.

Hendon, H., and M.L. Salby, 1994: The life cycle of the Madden-Julian oscillation. *J. Atmos. Sci.,* **51,** 2207-2219.

--------, and --------, 1996: Planetary-scale circulations forced by intraseasonal variations of observed convection. *J. Atmos. Sci.,* **53,** 1751-1758.

--------, and J. Glick, 1997: Intraseasonal air-sea interaction in the tropical Indian and Pacific Oceans. *J. Climate,* **10,** 647-661.

Hsu, H.H., and C.H Weng, 2001: Northwestward Propagation of the Intraseasonal Oscillation in the Western North Pacific during the Boreal Summer: Structure and Mechanism. *J. Climate*, **14,** 3834-3850.

Jiang, X., T. Li, and B. Wang, 2004: Structures and mechanisms of the northward propagating boreal summer intraseasonal oscillation. *J. Climate*, **17,** 1022-1039.

Julian, P.R., and R.A. Madden, 1981: Comments on a paper by T. Yasunari, "A quasi-stationary appearance of 30 to 40 day period in the cloudiness fluctuations during the summer monsoon over India". *J. Meteor. Soc. Japan,* **59,** 435-437.

Kalnay, E., and Co-authors, 1996: The NCEP/NCAR 40-year Reanalysis Project. *Bull. Amer. Meteor. Soc.,* **77,** 437-471.

Kang, I., and Co-authors, 2002: Intercomparison of the climatological variations of Asian summer monsoon precipitation simulated by 10 GCMs. *Climate Dyn.,* **19,** 383-395.

Kemball-Cook, S., and B. Wang, 2001: Equatorial waves and air-sea interaction in the boreal summer intraseasonal oscillation. *J. Climate,* **14,** 2923-2942.

--------, ---------, and X. Fu, 2002: Simulation of the intraseasonal oscillation in the ECHAM-4 Model: The impact of coupling with an ocean mode. *J. Atmos. Sci.,* **59,** 1433-1453.

Kim, K.Y., and G.R. North, 1997: EOFs of harmonizable cyclostationary processes. *J. Atmos. Sci.*, **54,** 2416-2427.

-------, and Q. Wu, 1999: A comparison study of EOF techniques: Analysis of nonstationary data with periodic statistics. *J. Climate,* **12,** 185-199.

-------, 2003: Investigation of ENSO variability using cyclostationary EOFs of observational data. *Meteor. Atmos. Phys.*, **81,** 149-168.

Krishnan, R., C. Zhang and M. Sugi, 2000: Dynamics of breaks in the Indian summer monsoon. *J. Atmos. Sci.,* **57,** 1354-1372.

Krishnamurti, T.N., and D. Subrahmanyam, 1982: The 30-50 day mode at 850 mb during MON-EX. *J. Atmos. Sci.,* **39,** 2088-2095.

---------, D. Dosterhof, and A. Mehta, 1988: Air-sea interaction on the time scale of 30-50 days. *J. Atmos. Sci.,* **45,** 1304-1322.

Krishnamurthy, V., and J. Shukla, 2000: Intraseasonal and interannual variability of rainfall over India. *J. Climate,* **13,** 4366-4377.

Lau, K.M., and P.H. Chan, 1986: Aspects of the 40-50 day oscillation during the northern summer as inferred from outgoing longwave radiation. *Mon. Wea. Rev.,* **114,** 1354-1367.

-------, and L. Peng, 1987: Origin of low frequency (intraseasonal) oscillations in the tropical atmosphere. Part I: Basic theory. *J. Atmos. Sci.,* **44** 950-972.

-------, and ------, 1990: Origin of low frequency (intraseasonal) oscillations in the tropical atmosphere. Part III: Monsoon dynamics. *J. Atmos. Sci.,* **47,** 1443-1462.

Lawrence, D. M., and P.J. Webster, 2002: The boreal summer intraseasonal oscillation: Relationship between northward and eastward movement of convection. *J. Atmos. Sci.,* **59,** 1593-1606.

Liebmann, B., H.H. Hendon, and J.D. Glick, 1994: The relationship between tropical cyclones of the western Pacific and Indian Ocean and Madden-Julian oscillation. *J. Meteor. Soc. Japan,* **72,** 401-412.

-------, and C. A. Smith, 1996: Description of a complete (interpolated) OLR dataset. *Bull. Amer. Meteor. Soc.*, **77,** 1275-1277.

Mapes, B.E., and R.A. Houze, 1995: Diabatic divergence profiles in western Pacific mesoscale convective system. *J. Atmos. Sci.,* **29,** 1109-1123.

Matsuno, T., 1966: Quasi-geostrophic motions in the equatorial area. *J. Meteor. Soc. Japan,* **44,** 25-42.

Murakami, T., T. Nakazawa, and J. He, 1984: On the 40-50 day oscillations during the 1979 Northern Hemisphere summer. I: Phase propagation. *J. Meteor. Soc. Japan,* **62,** 440-468.

Nanjundiah R S, J Srinivasan and S Gadgil, 1992: Intraseasonal variation of the Indian summer monsoon. II: Theoretical aspects. *J. Meteor. Soc. Japan,* **70,** 529-550.

Palmer, T.N., 1994: Chaos and predictability in forecasting the monsoon. *Proc. Indian. Natl. Sci. Acad.,* **60A,** 57-66.

Raghavan, K., 1973: Break-monsoon over India. *Mon. Wea. Rev.,* **101,** 33-43.

Rao, K.G., M. Desbois, and R. Roca, 2004: Upper tropospheric drying and the transition to break in the Indian summer monsoon during 1999. *Geophys. Res. Lett.,* **31,** L03206, doi:10.1029/2003GL018269, 2004.

Reed, R.J., and E.E. Recker, 1971: Structure and properties of synoptic-scale wave disturbances in the equatorial western Pacific. *J. Atmos. Sci.,* **28,** 1117-1133.

Reynolds, R. W., and T. M. Smith, 1994: Improved global sea surface temperature analyses using optimum interpolation. *J. Climate*, **7,** 929-948.

Rodwell, M.J., and B.J. Hoskins, 1996: Monsoons and the dynamics of deserts. *Quart.J.Roy. Meteor. Soc.,* **122,** 1385-1404.

Sengupta, D., B. N. Goswami and R. Senan, 2001: Coherent intraseasonal oscillations of the ocean and atmosphere during the Asian summer monsoon. *Geophys. Res. Lett.,* **28,** 21, 4127-4130.

Sikka, D.R., and S. Gadgil, 1980: On the maximum cloud zone and the ITCZ over Indian longitudes during the southwest Monsoon. *Mon. Wea. Rev.,* **108,** 1840-1853.

Sperber, K. R., 2003: Propagation and the vertical structure of the Madden-Julian oscillation. *Mon. Wea. Rev.,* **131,** 3018-3037.

------, J. M. Slingo, P. M. Inness, and W.-K. M. Lau, 1997: On the maintenance and initiation of the intraseasonal oscillation in the NCEP/NCAR reanalysis and in the GLA and UKMO AMIP simulations. *Climate. Dyn.,* **13,** 769-795.

------, ------, and H. Annamalai, 2000: Predictability and the relationship between subseasonal and interannual variability during the Asian summer monsoon. *Quart. J. Roy. Meteor. Soc.,* **126,** 2545-2574.

------, and Co-authors, 2001: Dynamical seasonal predictability of the Asian summer monsoon. *Mon. Wea. Rev,* **129,** 2226-2248.

Srinivasan, J., S. Gadgil, and P.J.Webster, 1993: "Meridional migration of large-scale monsoon convective zones", *Meteor. Atmos. Phys.*, **52,**15-35.

Sui, C.H., and K.M. Lau, 1989: Origin of low-frequency (intraseasonal) oscillations in the tropical atmosphere. Part II: Structure and propagation of mobile wave-CISK modes and their modification by lower boundary forcing. *J. Atmos. Sci.,* **46,** 38-56.

Ting, M., and L. Yu, 1998: Steady response to tropical heating in wave linear and nonlinear baroclinic model. *J. Atmos. Sci.,* **55,** 2509-2527.

Trenberth, K.E., and C.J. Guillemot, 1998: Evaluation of the atmospheric moisture and hydrological cycle in the NCEP/NCAR reanalyses. *Climate Dyn.,* **14,** 213-231.

Vecchi, G. A., and D.E. Harrison, 2002: Monsoon breaks and subseasonal sea surface temperature variability in the Bay of Bengal. *J. Climate,* **15,** 1485-1493.

Waliser, D.E., K.M. Lau and J.H. Kim, 1999: The influence of coupled sea surface temperatures on the Madden-Julian oscillation: A model perturbation experiment. *J. Atmos. Sci.,* **56,** 333-358.

-------, and Co-authors, 2004: AGCM simulations of intraseasonal variability associated with the Asian summer monsoon. *Climate. Dyn.,* **21,** 423-446.

Wang, B., and H. Rui, 1990: Synoptic climatology of transient tropical intraseasonal convection anomalies: 1975-1985. *Meteor. Atmos. Phys.,* **44,** 43-61.

------, and X. Xie, 1996: Low-frequency equatorial waves in vertically sheared zonal flow. Part II: Unstable waves. *J. Atmos. Sci.,* **53,** 3589-3605.

-------, and X. Xie, 1997: A model for the boreal summer intraseasonal oscillation. *J. Atmos. Sci.,* **54,** 72-86.

-------, 2004: Basic Theories, A Chapter in the Book "Intraseasonal variability of the ocean and atmosphere" Eds. K.M. Lau and D.E. Waliser (in press).

Watanabe, M., and M. Kimoto, 2000: Atmosphere-ocean thermal coupling in the north Atlantic: A positive feedback. *Quart. J. Roy. Meteor. Soc.,* **126,** 3343-3369.

-------, and ------, 2001: Corrigendum, *Quart. J. Roy. Meteor. Soc.,* **127,** 733-734.

--------, and F.F. Jin, 2002: Role of Indian Ocean warming in the development of Philippine Sea anticyclone during ENSO. *Geophys. Res. Lett,* **29,** 10.1029/2001GL014318.

-------, and ---------, 2003: A moist linear baroclinic model: Coupled dynamical-convective response to El Nino. *J. Climate,* **16,** 1121-1139.

Webster, P.J., 1972: Response of the tropical atmosphere to local steady forcing. *Mon. Wea. Rev.*, **100,** 518-541.

-------., 1983: Mechanisms of monsoon low-frequency variability: Surface hydrological effects. *J. Atmos. Sci.,* **40,** 2110-2124.

-------, V.O. Magana, T.N. Palmer, J. Shukla, R.A. Thomas, M. Yanai, and T. Yasunari, 1998: The monsoon: Processes, predictability and prediction. *J. Geophys. Res.,* **103,** 14451-14510.

Woolnough, S. J., J. M. Slingo and B. J. Hoskins, 2000: The relationship between convection and sea surface temperature on intraseasonal time scales. *J. Climate,* **13,** 2086-2104.

Wu, Z., E.S. Sarachik and D. Battisti, 2000: Vertical structure of convective heating and the three-dimensional structure of the forced circulation on an equatorial beta plane. *J. Atmos. Sci.,* **57**, 2169-2187.

Xie, P., and P. Arkin, 1996: Analyses of global monthly precipitation using gauge observations, satellite estimates, and numerical model predictions. *J. Climate,* **9,** 840-858.

Yasunari, T., 1979: Cloudiness fluctuations associated with the Northern Hemisphere summer monsoon. *J. Meteor. Soc. Japan,* **57,** 227-242.

--------., 1981: Structure of an Indian monsoon system with around 40-day period. *J. Meteor. Soc. Japan,* **59,** 336-354.

Figure Captions

Figure 1: June-September 1979-95 AVHRR OLR (a) climatological mean, (b) daily variance, (c) 20-100 day bandpass filtered variance, and (d) percent of daily variance explained by 20-100 day filtered data.

Figure 2: Cyclostationary EOF's of 20-100 day bandpass filtered AVHRR OLR for June-September 1979-95. The EOF's have been scaled by a one standard deviation of the PC's to give units of Wm^{-2}. (a) day -15, (b) day -10, (c) day -5, (d) day 0, (e) day 5, (f) day 10, (g) day 15, and (h) day 20.

Figure 3: For each summer (June-September 1979-95) the percent variance of observed all-India rainfall (AIR) departures explained by PC-4 as determined from lagged correlation analysis. The daily observed AIR departures were smoothed with a 9-day running mean prior to the analysis. The horizontal line corresponds to the 5% significance level assuming 12 degrees of freedom.

Figure 4: Linear regressions of PC-4 with 20-100 day bandpass filtered CMAP rainfall (mm day^{-1}) and NCEP/NCAR Reanalysis 850hPa wind (a) day -15, (b) day -10, (c) day -5, (d) day 0, (e) day 5, (f) day 10, (g) day 15, and (h) day 20. Data is plotted where the regression is significant at the 5% level or better assuming each pentad is independent. All regressions have been scaled by a 1 standard deviation perturbation of PC-4 to give the afore-mentioned units.

Figure 5: Day -15 (a) Column integrated heating anomalies ($^oC\ day^{-1}$), Steady-state response of 850hPa wind (ms^{-1}) and divergence (s^{-1}) to day -15 heating: (b) negative heating over the equato-

rial Indian Ocean, (c) positive heating over the tropical west Pacific, and (d) total response [sum of (b) and (c)].

Figure 6: Day -15 linear regressions of PC-4 with 20-100 day bandpass filtered (a) SST and surface temperature (^{o}C) and surface wind (ms^{-1}), (b) latent heat flux (Wm^{-2}) and surface wind stress (Nm^{-2}), (c) 1000hPa divergence (s^{-1}), and (d) 850hPa specific humidity (kg kg^{-1}). Significance testing and scaling as in Fig. 4.

Figure 7: Day 10 linear regressions of PC-4 with 20-100 day bandpass filtered (a) CMAP rainfall (mm day^{-1}) and 850hPa wind (ms^{-1}), (b) SST and surface temperature (^{o}C) and surface wind (ms^{-1}), (c) 850hPa specific humidity (kg kg^{-1}), (df) as (a-c) but for day 20. Significance testing and scaling as in Fig. 4.

Figure 8: Steady-state response of 850hPa wind (ms^{-1}) and relative vorticity (s^{-1}) to day 10 heating. (a) positive heating over the Bay of Bengal, (b) positive heating over the equatorial west Pacific, (c) negative heating over the tropical west Pacific, and (d) total response [sum of (a), (b), and (b)].

Figure 9: Steady-state response of 850hPa wind (ms^{-1}) and relative vorticity (s^{-1}) to day 20 (a) positive heating over the tropical west Pacific, (b) all heatings, and (c) vertical profile of anomalous vertical velocity (ω, hPa s^{-1}) averaged over India (70^{o}-100^{o}E, 10^{o}-25^{o}N) based on north tropical west Pacific heating (closed circles) and negative heating over the equatorial Indian Ocean (open circles). Positive (negative) values correspond to descent (ascent).

Figure 10: Linear regressions of PC-4 with 20-100 day bandpass filtered specific humidity (kg kg^{-1}) at 92.5^{o}E, averaged between 15^{o}N-20^{o}N, from 1000hPa to 300hPa as a function of time lag (-25 to 25 days). Significance testing and scaling as in Fig. 4.

Figure 11: Temporal evolution of 700hPa geopotential height anomalies (m) for day 20 positive heating over the tropical west Pacific. (a) day 3, (b) day 6, (c) day 9, and (d) day 12.

Figure 12: As Fig. 10 but for day 20 negative heating over the equatorial Indian Ocean.

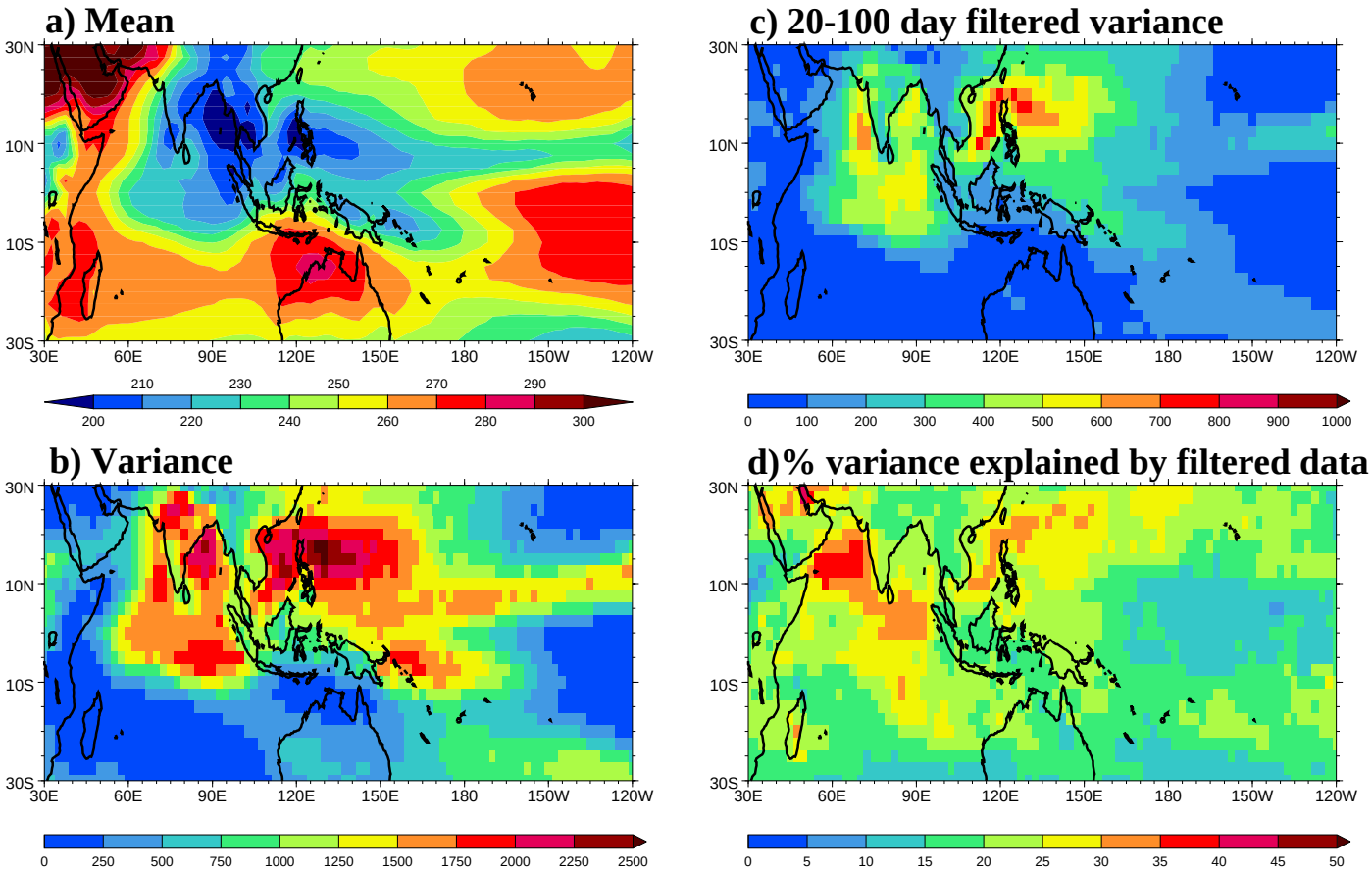

Figure 1: June-September 1979-95 AVHRR OLR (a) climatological mean, (b) daily variance, (c) 20-100 day bandpass filtered variance, and (d) percent of daily variance explained by 20-100 day filtered data.

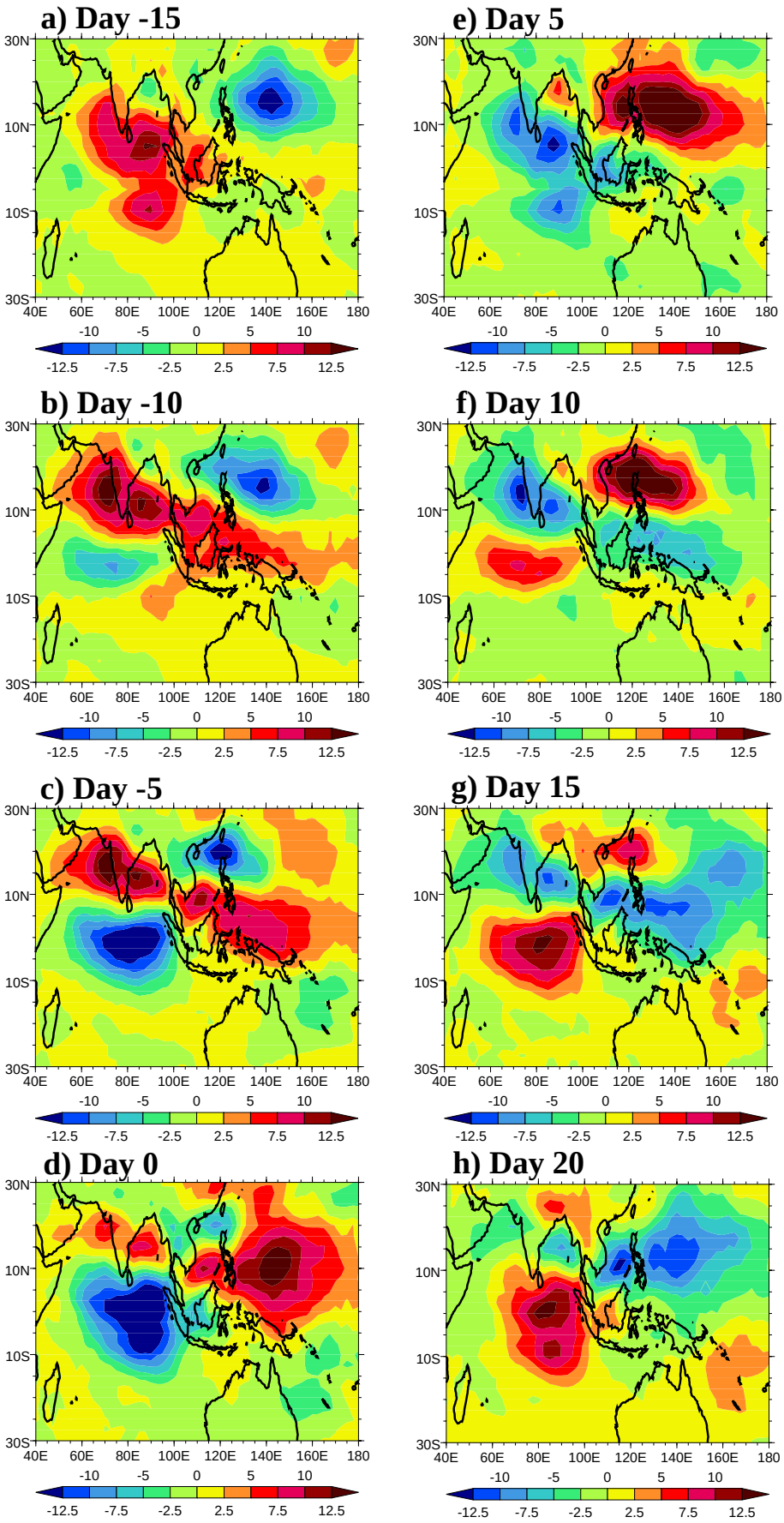

Figure 2: Cyclostationary EOF's of 20-100 day bandpass filtered AVHRR OLR for June-September 1979-95. The EOF's have been scaled by a one standard deviation of the PC's to give units of Wm^{-2}. (a) day -15, (b) day -10, (c) day -5, (d) day 0, (e) day 5, (f) day 10, (g) day 15, and (h) day 20.

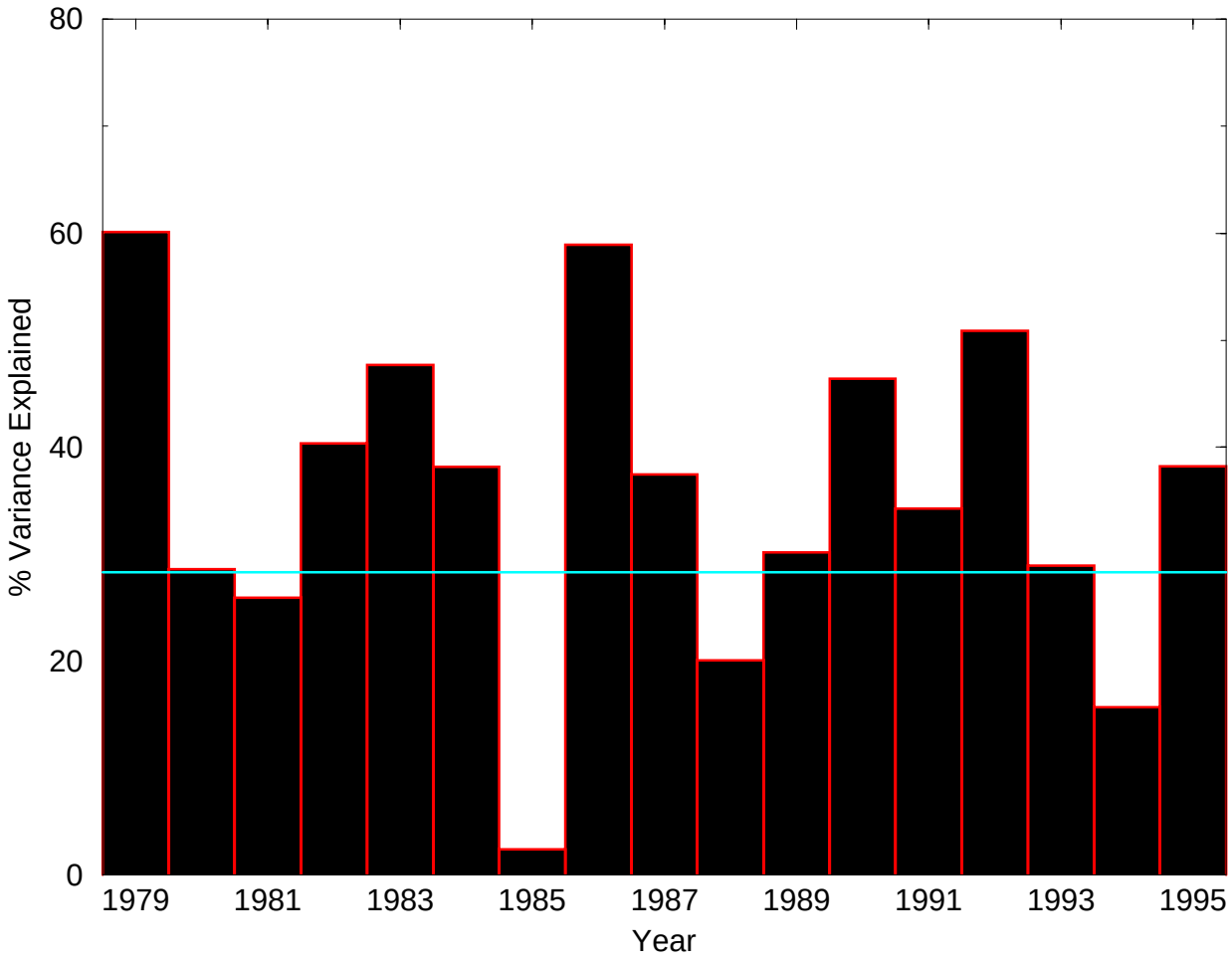

Figure 3: For each summer (June-September 1979-95) the percent variance of observed all-India rainfall (AIR) departures explained by PC-4 as determined from lagged correlation analysis. The daily observed AIR departures were smoothed with a 9-day running mean prior to the analysis. The horizontal line corresponds to the 5% significance level assuming 12 degrees of freedom.

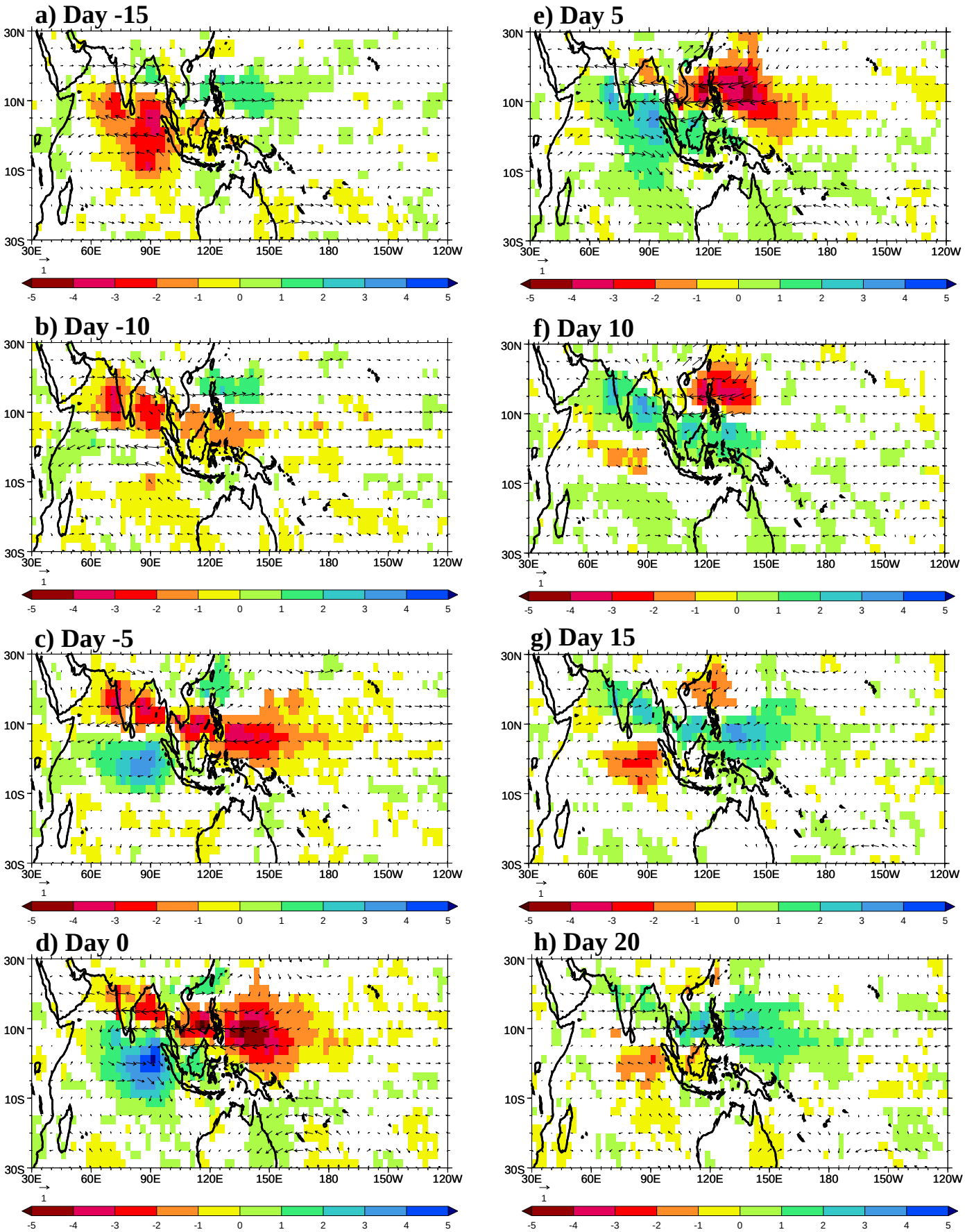

Figure 4: Linear regressions of PC-4 with 20-100 day bandpass filtered CMAP rainfall (mm day^{-1}) and NCEP/NCAR Reanalysis 850hPa wind (a) day -15, (b) day -10, (c) day -5, (d) day 0, (e) day 5, (f) day 10, (g) day 15, and (h) day 20. Data is plotted where the regression is significant at the 5% level or better assuming each pentad is independent. All regressions have been scaled by a 1 standard deviation perturbation of PC-4 to give the afore-mentioned units.

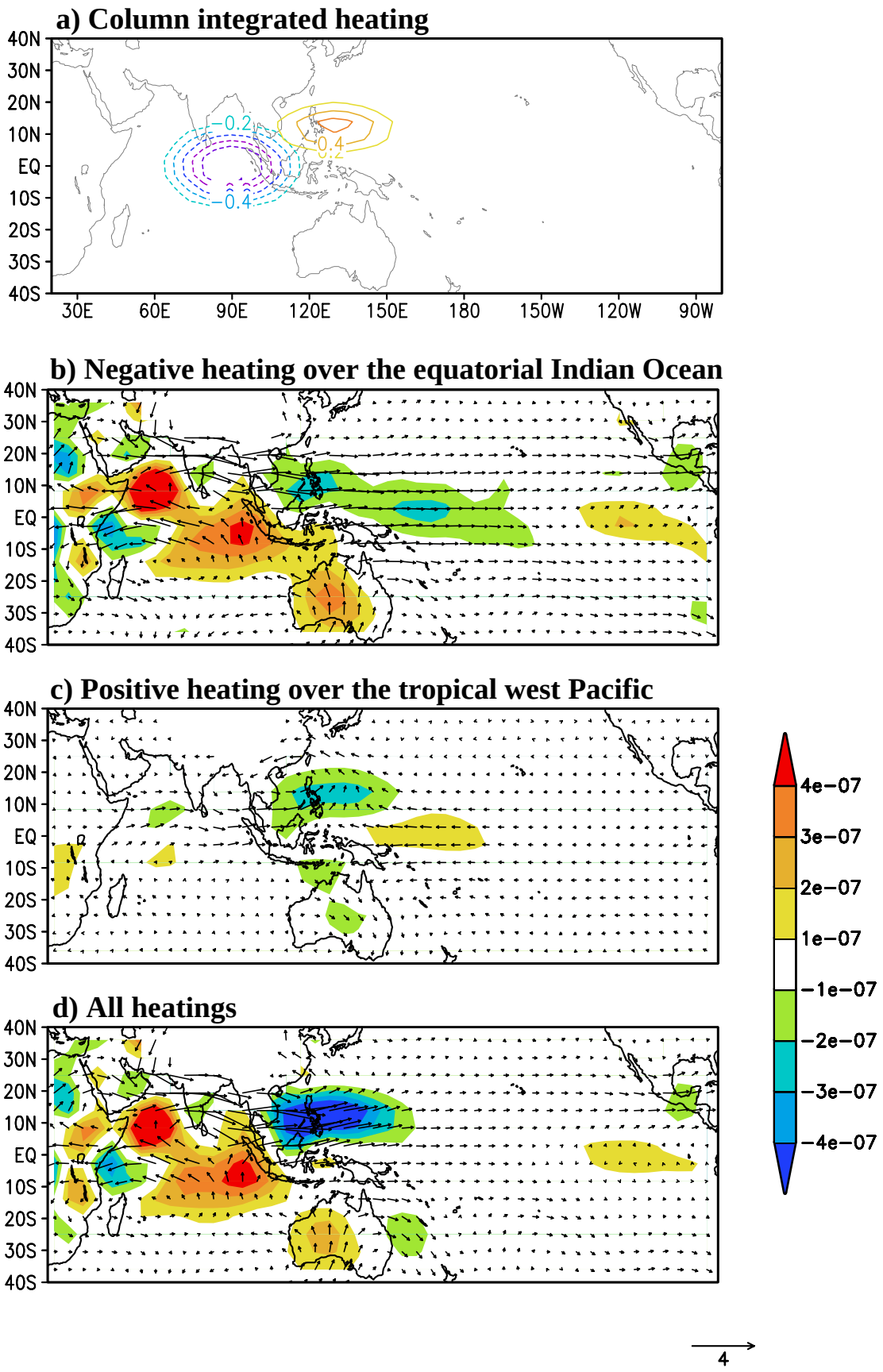

Figure 5: Day -15 (a) Column integrated heating anomalies (^{o}C day^{-1}), Steady-state response of 850hPa wind (ms^{-1}) and divergence (s^{-1}) to day -15 heating: (b) negative heating over the equatorial Indian Ocean, (c) positive heating over the tropical west Pacific, and (d) total response [sum of (b) and (c)].

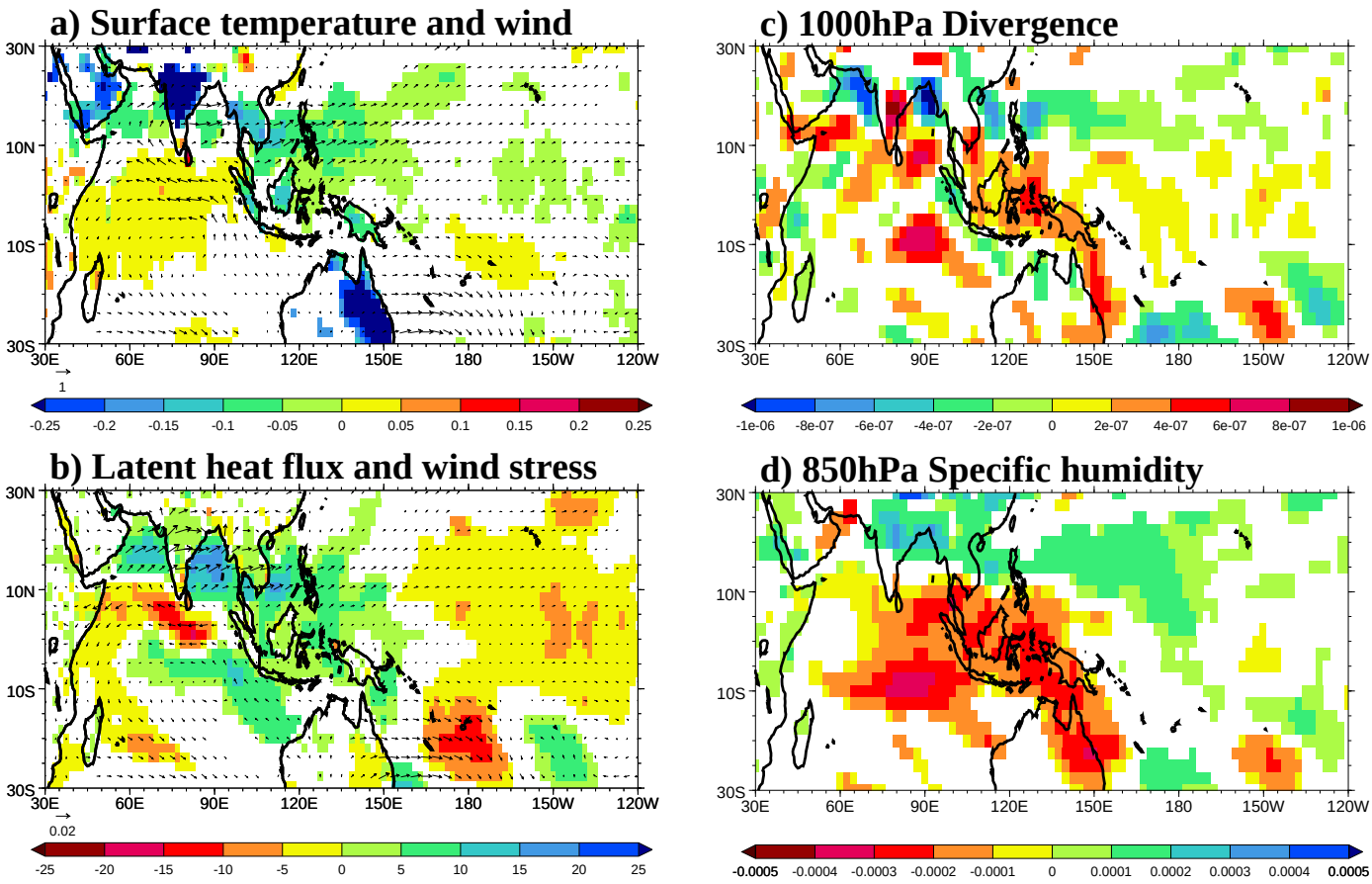

Figure 6: Day -15 linear regressions of PC-4 with 20-100 day bandpass filtered (a) SST and surface temperature (^{o}C) and surface wind (ms^{-1}), (b) latent heat flux (Wm^{-2}) and surface wind stress (Nm^{-2}), (c) 1000hPa divergence (s^{-1}), and (d) 850hPa specific humidity (kg kg^{-1}). Significance testing and scaling as in Fig. 4.

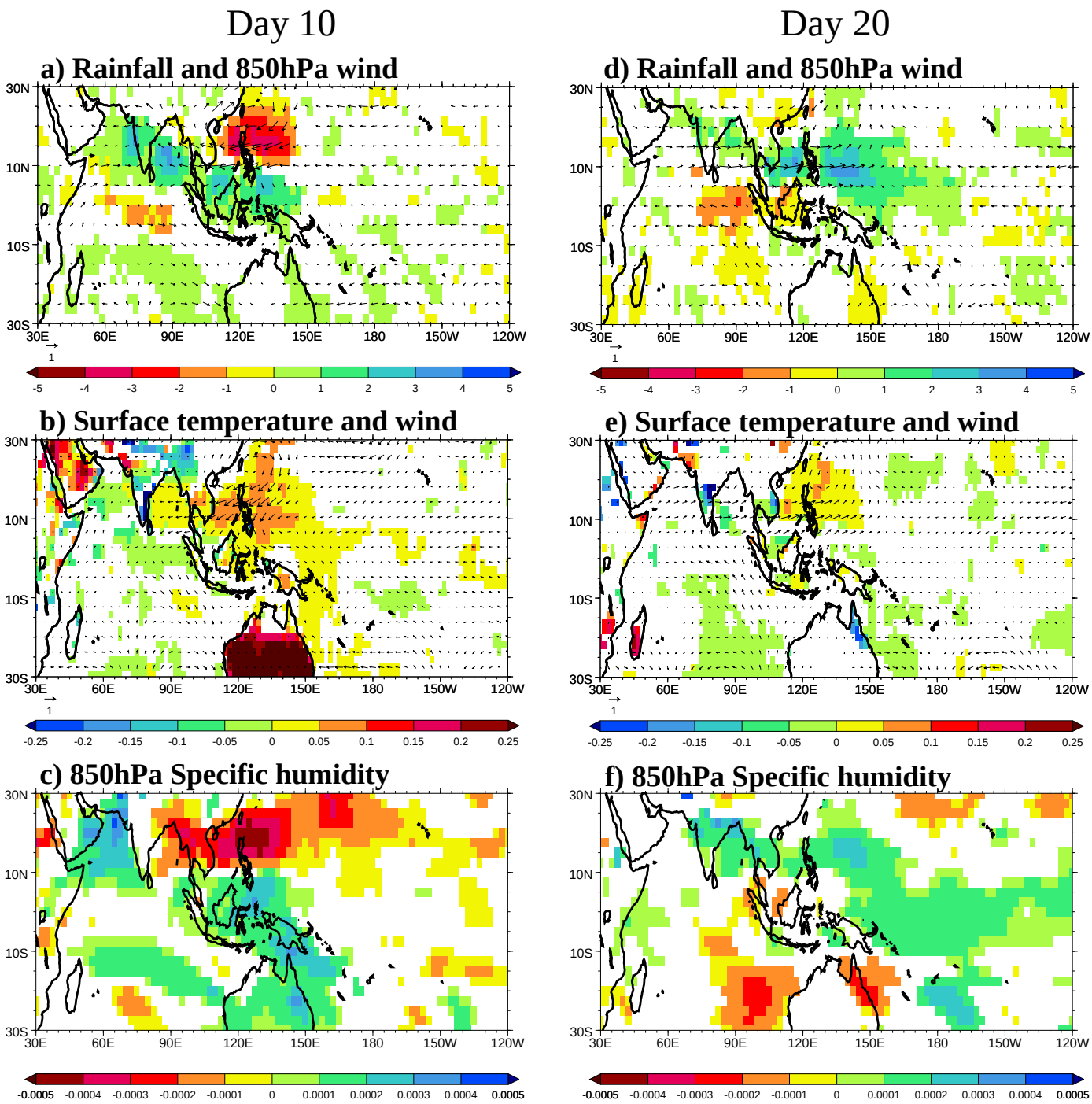

Figure 7: Day 10 linear regressions of PC-4 with 20-100 day bandpass filtered (a) rainfall (mm day^{-1}) and 850hPa wind (ms^{-1}), (b) SST and surface temperature (^{o}C) and surface wind (ms^{-1}), (c) 850hPa specific humidity (kg kg^{-1}), (df) as (a-c) but for day 20. Significance testing and scaling as in Fig. 4.

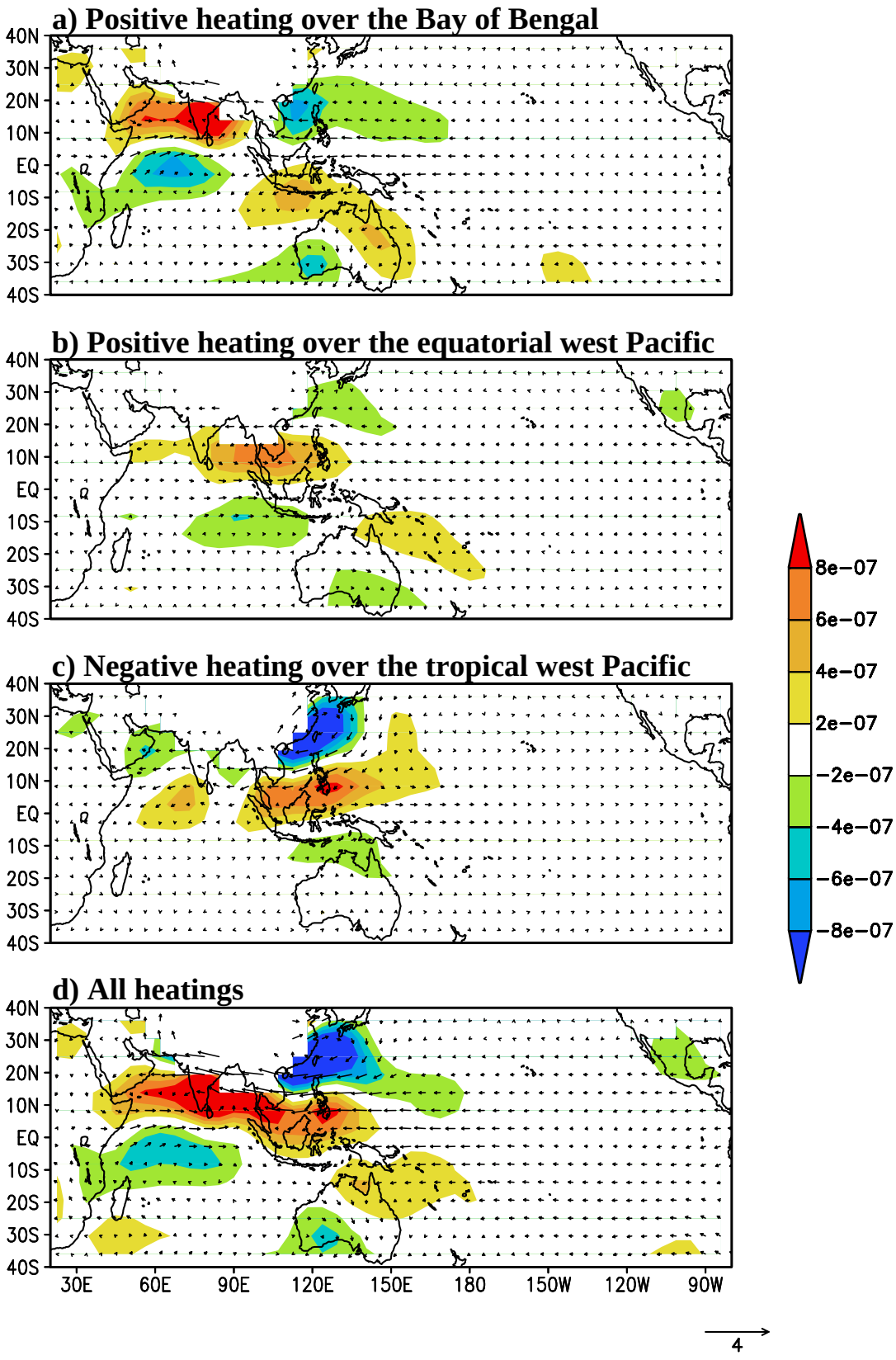

Figure 8: Steady-state response of 850hPa wind (ms^{-1}) and relative vorticity (s^{-1}) to day 10 heating. (a) positive heating over the Bay of Bengal, (b) positive heating over the equatorial west Pacific, (c) negative heating over the tropical west Pacific, and (d) total response [sum of (a), (b), and (b)].

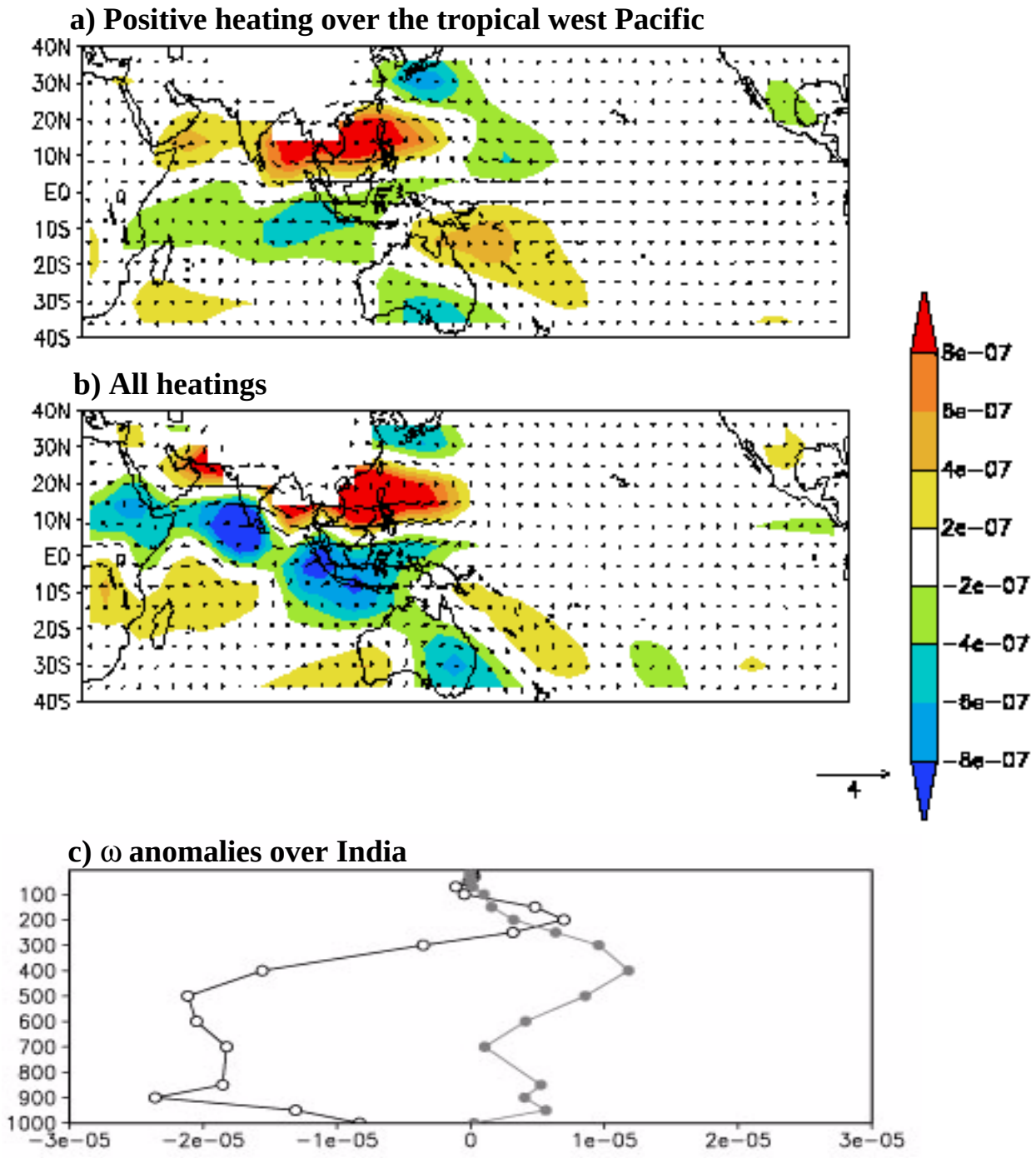

Figure 9: Steady-state response of 850hPa wind (ms^{-1}) and relative vorticity (s^{-1}) to day 20 (a) positive heating over the tropical west Pacific, (b) all heatings, and (c) vertical profile of anomalous vertical velocity (ω, hPa s^{-1}) averaged over India (70^{o}-100^{o}E, 10^{o}-25^{o}N) based on north tropical west Pacific heating (closed circles) and negative heating over the equatorial Indian Ocean (open circles). Positive (negative) values correspond to descent (ascent).

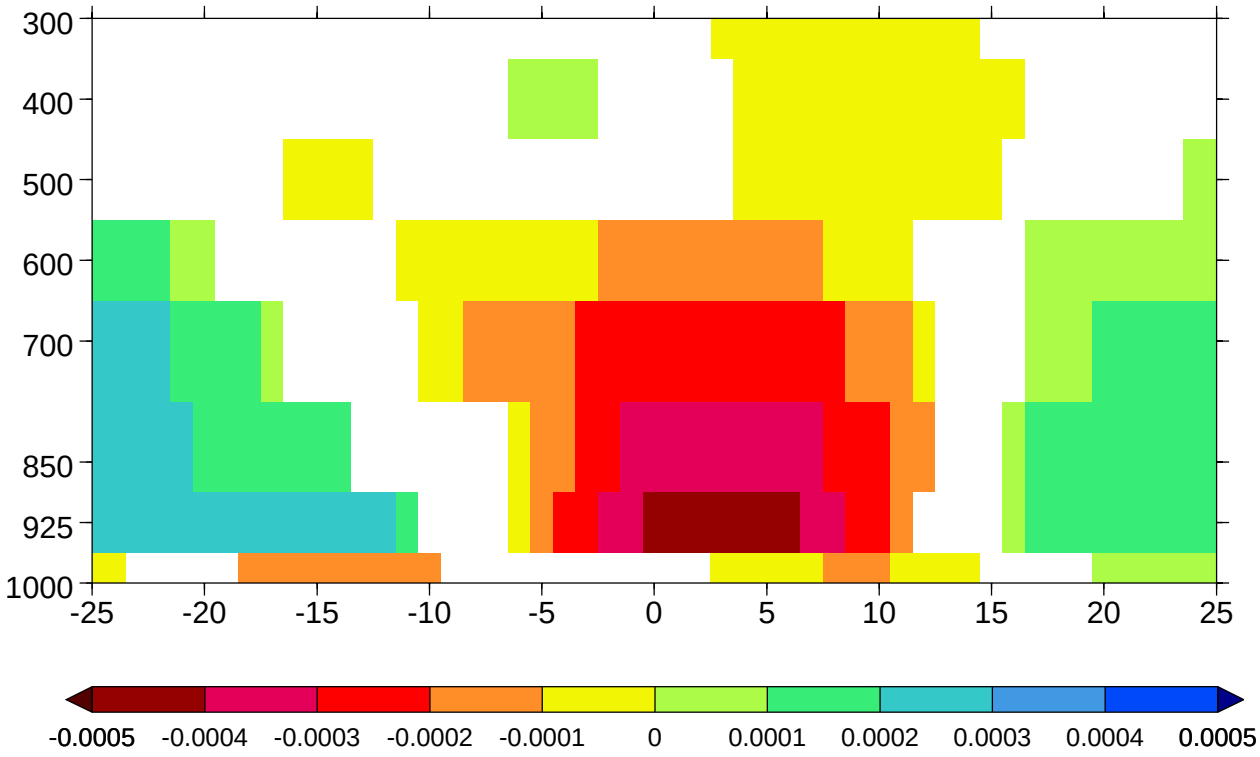

Figure 10: Linear regressions of PC-4 with 20-100 day bandpass filtered specific humidity (kg kg^{-1}) at 92.5^{o}E, averaged between 15^{o}N-20^{o}N, from 1000hPa to 300hPa as a function of time lag (-25 to 25 days). Significance testing and scaling as in Fig. 4.

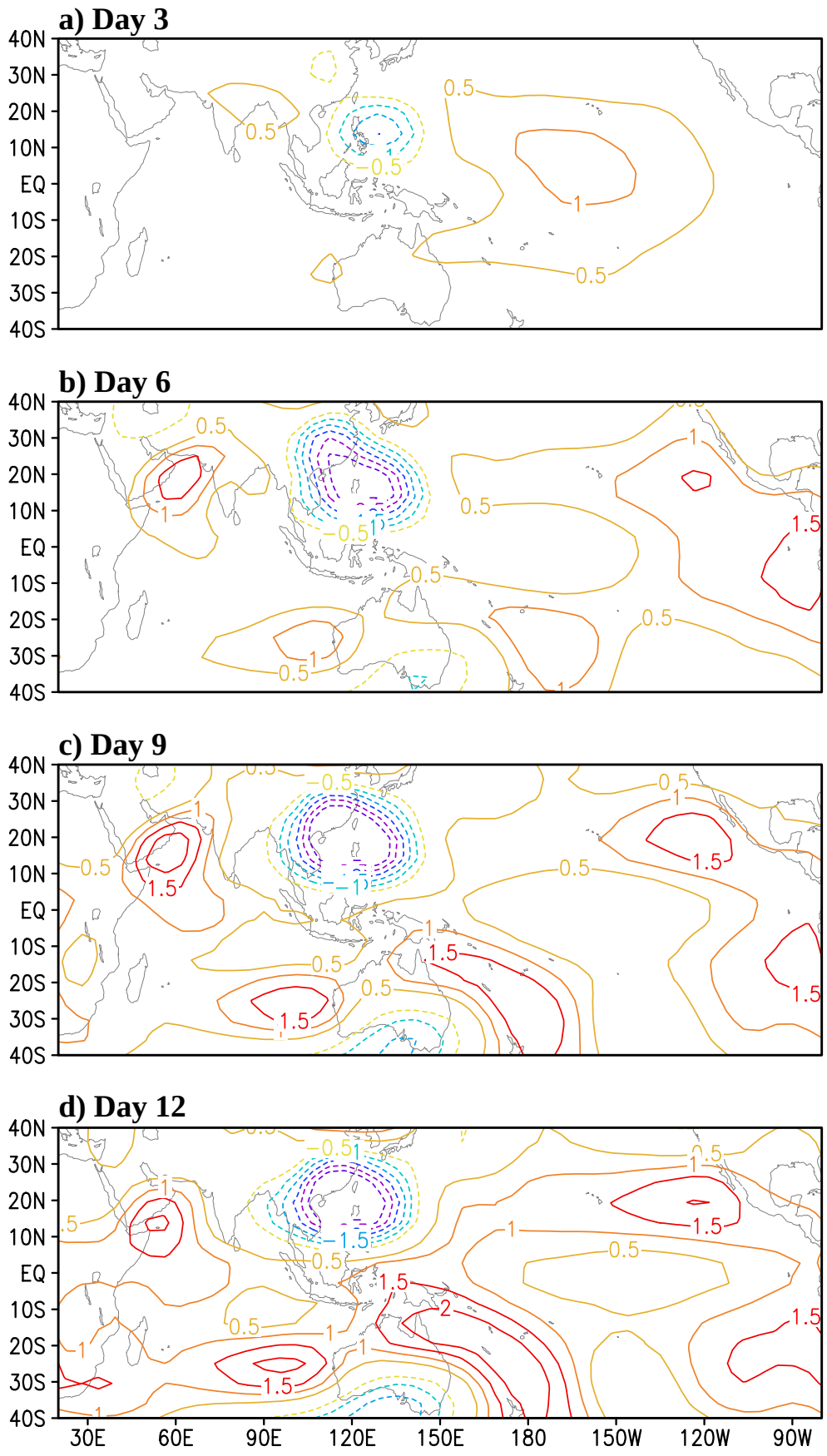

Figure 11: Temporal evolution of 700hPa geopotential height anomalies (m) for day 20 positive heating over the tropical west Pacific. (a) day 3, (b) day 6, (c) day 9, and (d) day 12.

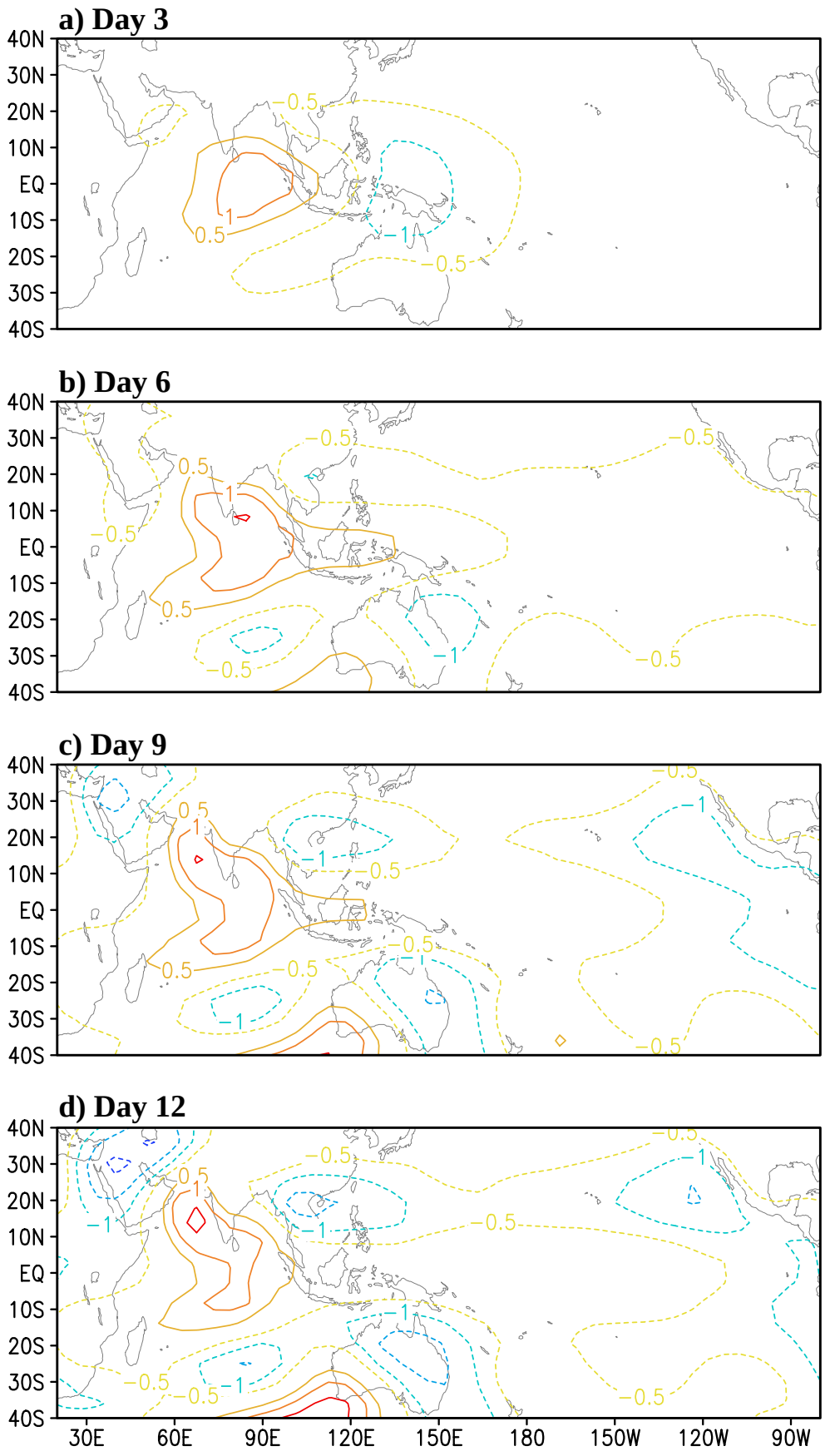

Figure 12: As Fig. 11 but for day 20 negative heating over the equatorial Indian Ocean.